

Journal of Materials Chemistry A

Materials for energy and sustainability

Accepted Manuscript

This article can be cited before page numbers have been issued, to do this please use: B. C. Tapia, J. Y. Yeo and Z. Smith, *J. Mater. Chem. A*, 2026, DOI: 10.1039/D5TA09448H.



This is an Accepted Manuscript, which has been through the Royal Society of Chemistry peer review process and has been accepted for publication.

Accepted Manuscripts are published online shortly after acceptance, before technical editing, formatting and proof reading. Using this free service, authors can make their results available to the community, in citable form, before we publish the edited article. We will replace this Accepted Manuscript with the edited and formatted Advance Article as soon as it is available.

You can find more information about Accepted Manuscripts in the [Information for Authors](#).

Please note that technical editing may introduce minor changes to the text and/or graphics, which may alter content. The journal's standard [Terms & Conditions](#) and the [Ethical guidelines](#) still apply. In no event shall the Royal Society of Chemistry be held responsible for any errors or omissions in this Accepted Manuscript or any consequences arising from the use of any information it contains.

Computational and experimental insights into variable temperature propylene (C_3H_6), propane (C_3H_8), and hydrogen sulfide (H_2S) sorption in ultra-high permselectivity CANAL ladder polymers

Brandon C. Tapia¹, Jing Ying Yeo¹, and Zachary P. Smith^{*1}

¹Department of Chemical Engineering, Massachusetts Institute of Technology, Cambridge, Massachusetts 02139, USA

*Corresponding author: Zachary P. Smith (zpsmith@mit.edu)

Abstract

Membranes are a promising technology for energy-efficient separations of high-value gaseous chemical streams (e.g., hydrogen sulfide from methane or propane from propylene). Among the classes of emerging microporous polymers, CANAL polymers have attracted significant interest because of their selectivities and plasticization resistance for acid gas separations. In this work, a computational atomistic system is developed for CANAL-Me-Me₂F, an archetypal CANAL polymer. Computed properties (free volume distribution, wide-angle X-ray scattering, and thermal expansion coefficients) align with experimental results. High-pressure sorption isotherms of H₂, N₂, O₂, CH₄, CO₂, H₂S, C₃H₆, and C₃H₈ were computed via grand canonical Monte Carlo and iterated Monte Carlo–molecular dynamics simulations, demonstrating good agreement with experimental isotherms at 35 °C. H₂S, C₃H₆, and C₃H₈ isotherms were further computed between temperatures of 55–190 °C, followed by extraction of dual-mode sorption (DMS) parameters. Sorption energetics showed less exothermic Langmuir affinity for the more polarizable gases (H₂S and C₃H₆) in CANAL-Me-Me₂F relative to PIM-1, which is ascribed to the lack of heteroatoms in CANAL-Me-Me₂F, and supported by simulations of a hypothetical nitrile-functionalized CANAL-Me-Me₂F. This study develops a computational approach that can probe the unique nanoscale behavior of CANAL polymers and applies it to studying the thermodynamics of condensable gas sorption within CANAL-Me-Me₂F.



1. Introduction

Reducing energy consumption in chemical separations is an important industrial target that can address up to 15% of global energy use.¹ One potential route to achieving this goal is transitioning from conventional thermal-based separations to membrane-based systems, which leverage chemical potential gradients to separate compounds based upon their size and affinity to the membrane.²

Ladder polymers are a promising class of emerging materials with highly rigid and contorted backbones, among which, the best known are polymers of intrinsic microporosity (PIMs).³ These materials have inefficient chain packing, yielding interconnected free volume elements that allow an increase in permeability while maintaining moderate selectivity.³ Nevertheless, the out-of-equilibrium glassy structure of PIMs results in a loss of free volume with time, decreasing their permeability that would benefit industrial application.^{3,4} Thus, significant work has been devoted to developing microporous membranes that can mitigate physical aging.³

In 2022, Lai et al.⁵ reported a class of 3D-contorted ladder polymers made via catalytic arene–norbornene annulation (CANAL) polymerization, comprised of fused norbornyl benzocyclobutene repeat units. These CANAL polymers exhibited molecular weights between 67 and 170 kDa, suitable for forming mechanically and thermally robust gas separation membranes. Interestingly, CANAL polymers exhibit a unique physical aging trend that does not follow the upper bound relationship. Instead, selectivity is greatly increased while permeability does not suffer significantly for small molecules, unlike the commonly observed tradeoff in other membrane materials, including traditional PIMs.^{3,6,7} This aging behavior allows for CANAL polymers to rival industrially used membranes in selectivity while significantly surpassing them in permeability. For example, the CANAL polymer studied in this work, CANAL-Me-Me₂F, exhibits twice the selectivity and 100 times the permeability of industrial cellulose acetate membranes for CO₂/CH₄ separations after 150 days of aging.⁵



Considering these prior promising results, this study examines sorption of gas streams containing propylene (C_3H_6) and propane (C_3H_8), and hydrogen sulfide (H_2S) in CANAL-Me-Me₂F. These gases were selected due to their industrial relevance and the typical challenges in accessing experimental data for these gases. Propylene is an essential feedstock for plastic production, but the generation of propylene, largely via thermal cracking, also generates propane which must be removed.^{1,8,9} This separation is challenging due to similar boiling points (C_3H_6 : $-47.62\text{ }^{\circ}C$, C_3H_8 : $-42.11\text{ }^{\circ}C$) and van der Waals diameters (C_3H_6 : 4.0 \AA , C_3H_8 : 4.2 \AA) of the gases, leading to a highly energy-intensive distillation process.^{10–12} Hydrogen sulfide is another component that must be removed from hydrocarbon streams due to both its toxicity and ability to poison catalysts, especially as lower-quality feedstocks become economically feasible.¹³ Industrially mature fuel-gas sweetening relies on either cryogenic distillation or absorption depending on the target application (i.e., liquid or gaseous product).^{14,15} However, these methods must overcome enthalpies of condensation or leverage toxic solvents during operations, respectively. These unwanted features are not found in membrane separations.^{1,16,17}

Due to the exceptional microporosity of CANAL polymers, which exhibit some of the highest BET surface areas of polymers reported in literature, they are expected to exhibit high sorption capacities despite their lack of heteroatoms.⁵ However, sorption studies on olefins, paraffins, and acid gases, while highly desirable, remain limited in the open literature.^{18,19} To the best of our knowledge, there has only been one study by Yeo et al.²⁰ focusing on H_2S separations in CANALs, and none focusing on olefin/paraffin applications. Moreover, H_2S -focused studies are also limited for the archetypal PIM (PIM-1) and its derivatives.^{21–24} There are likely two main reasons for this lack of H_2S -focused work in the literature: (1) H_2S is a highly toxic gas, limiting capabilities in academic labs to consider these experiments, and (2) gathering experimental sorption data is time consuming, especially for gases such as H_2S and condensable hydrocarbons with high sorption capacity. Additionally, many experimental systems are limited to temperature ranges that may be inadequate for industrial applications. Nevertheless, these studies are necessary to understand the thermodynamic behavior of these complex mixtures and to evaluate their



potential in gas separations, especially as sorption selectivity can be more indicative of membrane performance relative to diffusion selectivity for highly sorbing gases, such as H₂S-containing mixtures.¹⁸ Specifically, sorption analyses help to characterize polymer–gas affinity, predict effects of competitive sorption, and quantify polymer–gas energetics. As a result, these measurements are vital tools that can be used to investigate whether CANALs are a feasible materials platform for various gas separations.

Simulations provide an important complement to experiments. They can probe nanostructure relationships and conditions inaccessible to experimental methods and can provide high throughput studies to identify promising candidates for future experimental synthesis and studies. In an effort to add to the presently limited literature on sour gas and olefin/paraffin separations in high free volume polymers, we present here a combined experimental and computational study of C₃H₆, C₃H₈, and H₂S sorption within CANAL-Me-Me₂F.

We validate this framework by first comparing our results to experimentally measured properties (density, wide-angle X-ray scattering, free volume distribution, and sorption isotherms), followed by simulating experimental properties that are typically inaccessible, namely sorption and associated energetics for C₃H₆, C₃H₈, and H₂S at temperatures of 35 °C, 55 °C, 125 °C, and 190 °C.

2. Background and Theory

The sorption–diffusion model is commonly applied to describe gas transport in polymeric membranes, where P is the permeability, D is the effective diffusion coefficient, and S is the effective sorption coefficient:²

$$P = D \cdot S \quad (1)$$

The sorption coefficient can be calculated from sorption experiments as

$$S = \frac{C}{f} \quad (2)$$



where C is the concentration of gas sorbed ($\text{cm}_{\text{STP}}^3 \text{ cm}_{\text{pol}}^{-3}$) in the membrane in equilibrium with the gas phase at fugacity f (atm). Pure-gas sorption in glassy polymers is frequently modeled via the dual-mode sorption (DMS) model:^{25–27}

$$C = k_D f + \frac{C'_H b f}{1 + b f} \quad (3)$$

where k_D is Henry's constant ($\text{cm}_{\text{STP}}^3 \text{ cm}_{\text{pol}}^{-3} \text{ atm}^{-1}$), C'_H is the Langmuir capacity constant ($\text{cm}_{\text{STP}}^3 \text{ cm}_{\text{pol}}^{-3}$), and b is the Langmuir affinity constant (atm^{-1}). The DMS model views sorption in a polymer as the simple addition of sorption in hypothetical Langmuir and Henry modes, which are said to dominate partitioning at low and high pressures, respectively.²⁵

The sorption selectivity ($\alpha_{i/j}^S$) for one gas over another is defined by the ratio of their respective sorption coefficients:

$$\alpha_{i/j}^S = \frac{S_i}{S_j} = \frac{C_i}{f_i} / \frac{C_j}{f_j} \quad (4)$$

Ideal sorption selectivity refers to the sorption selectivity calculated based on the ratio of the pure-gas sorption coefficients. However, attempting to infer mixed-gas sorption from pure-gas experiments is challenging, especially for condensable gases, which not only preferentially exclude less condensable gases from sorbing but also plasticize the polymer matrix.^{18,20} One method to address this behavior is by using the adjusted DMS model by Koros et al.,²⁸ who extended the applicability of the DMS model to predict mixed-gas sorption of component i in an n -component mixture from pure-gas sorption data by accounting for competition between penetrants for a finite region of Langmuir sorption:

$$C_{i,\text{mixed}} = k_{D,i} f_i + \frac{C'_{H,i} b_i f_i}{1 + b_i f_i + \dots + b_n f_n} \quad (5)$$

As there may be multiple solutions to the DMS model with similar goodness of fits as shown by Ricci et al.,²⁹ extracting physically meaningful results from the parameters requires additional constraints within the optimization procedure. One class of constraints are linear free energy relationships (LFERs) applied to the DMS fitting procedure as developed by Wu et al.³⁰

In the limit of infinite dilution, sorption can be decoupled into Langmuir and Henry mode sorption as:



$$S_{\infty} = \lim_{f \rightarrow 0} \frac{C_i}{f_i} = S_{\infty, Henry} + S_{\infty, Langmuir} = k_{D,i} + C'_{H,i} b_i \quad (6)$$

As sorption is an equilibrium process, it can be further described via a Gibbs free energy relationship and subsequently separated into an entropic prefactor ($S_{\infty,0}$) coupled with an enthalpic van't Hoff temperature dependence:

$$S_{\infty} = S_{\infty,0} \exp\left(-\frac{\Delta H_{S,\infty}}{RT}\right) \quad (7)$$

where $\Delta H_{S,\infty}$ is the infinite dilution heat of sorption.^{30–32} Likewise, the same approach can be applied to the Henry and Langmuir sorption modes independently to extract the heats of Henry sorption (ΔH_D)

$$k_D = k_{D,0} \exp\left(-\frac{\Delta H_D}{RT}\right) \quad (8)$$

and Langmuir sorption (ΔH_b)

$$b = b_0 \exp\left(-\frac{\Delta H_b}{RT}\right) \quad (9)$$

where $k_{D,0}$ and b_0 are again entropic prefactors.^{30,33}

3. Computational Methods

3.1 Simulated Polymerization Technique

Simulating polymer structures to extract physically meaningful property sets is challenging, primarily due to their amorphous nature and the limited chain lengths that can be accessed with simulations.³⁴ Unlike crystalline and other ordered structures (e.g., metal–organic frameworks), amorphous polymers do not have periodic structures that can be readily compiled. Ladder polymers and PIMs bring the additional challenge of high steric hindrance due to their bulky structures.³⁵ Thus, traditional polymer building methods such as random walks, reverse Monte Carlo (RMC), or configurational bias Monte Carlo (CBMC) methods frequently fail to properly reduce the energy of the system or reproduce experimentally observed steric hindrance.^{34,35} To overcome these issues, simulated polymerization was employed here using the open-source Polymatic polymerization algorithm and software (version 1.1).^{34,36} Briefly, the Polymatic technique



places all monomers within a simulation box. Next, attempts are made to find bonding candidates based upon distance and orientation between potential bonding atoms. Should no candidates for polymerization be found, molecular dynamics are employed to search for more favorable bonding positions. Polymatic is extensively described in literature and has been validated with multiple polymers, including the archetypal microporous polymer, PIM-1.^{34,35,37–40}

The standard energy minimization strategy within the Polymatic algorithm was employed where canonical (NVT) molecular dynamics were performed every 5 polymerization steps except for when isothermal–isobaric (NPT) molecular dynamics were employed every 15 polymerization steps.³⁴ Additional bonding orientation constraints were employed to reduce unrealistic bond generation. Artificial charges of 0.3 e[±] were added to bonding atoms to increase bonding probability but removed once bonding was finalized. These orientation constraints and artificial charges are built into Polymatic and have been used previously for PIM-1.³⁴

3.2 Polymer Relaxation

After polymerization, CANAL-Me-Me₂F underwent a molecular dynamics relaxation scheme to more closely reflect its morphology under experimental conditions. To achieve this result, a 21-step equilibration algorithm was used where the pressure was stepped up in increments and then gradually reduced (**Figure S1** and **Table S1**) as recommended by Abbot et al.³⁴ This 21-step technique was developed based on the initial work of Theodorou and Suter and modified by Larsen et al.^{35,41} Molecular dynamics were performed with LAMMPS (version 22 Aug 2018 for pre-processing steps and version 28 Mar 2023 for sorption isotherms).⁴²

3.3 Simulation Parameters

Two separate systems were developed. The first was a united-atom (UA) framework defined by the General Amber Force Field 2 (GAFF2) force field for intramolecular energies and the Transferable Potential for Phase Equilibria United-Atom (TraPPE-UA) force field for intermolecular energies as was



previously shown to apply well for PIMs.^{34,37–39,43–49} In this UA technique, hydrogens are coupled with their respective heavy atoms, forming pseudoatoms. The second system was an all-atom (AA) framework defined by the GAFF2 force field for both inter- and intramolecular energies.⁴⁶ Partial charges were generated using the restrained electrostatic potential (RESP) approach at the HF/6-31G(d) level using the Connolly surface algorithm in Gaussian 16 via the PyRed program.^{50–55} To quantify charges, a single repeat unit model was used, except on bonding atoms where two joined repeat units were used instead so that the charges on bonding atoms could be better described. This method of using polymer periodicity has been previously applied in charge fitting and force field parameterization as polymers are generally too large to feasibly fit quantum-mechanically-derived charges to the entire chain.^{43,56–58} Charge tail corrections were included up to 15 Å and cross-charges were calculated using the Lorentz–Berthelot mixing rules.⁵⁹ The particle–particle–particle mesh (PPPM or P3M) method with a desired relative error (“accuracy”) of 10^{-5} was used to calculate long-range Coulombic interactions.⁶⁰ A Nosé–Hoover thermostat and barostat^{61–64} were employed with Störmer–Verlet integration.^{65,66} All penetrants were modeled as rigid bodies. All penetrants except for H₂ and H₂S used the GAFF2 and TraPPE-UA force fields for inter- and intramolecular energies, respectively. The H₂ force field was modeled using the parameters of Yang and Zhong,⁶⁷ as suggested for use by Barraco et al.⁶⁸ The H₂S force field was modeled using a modified 4-3 model originally developed by Shah et al.⁶⁹ Additional information on the H₂S force field is available in Section S1.3 of the Supplemental Information (SI).

3.4 Fixed and Flexible Adsorption Techniques

Grand canonical Monte Carlo (GCMC) simulations were employed to generate adsorption isotherms using the Cassandra Monte Carlo package (version 1.2.6).⁷⁰ GCMC holds chemical potential (μ), volume (V), and temperature (T) constant. Both a rigid and a flexible method were employed for sorption isotherm generation. The rigid method solely employed GCMC with the polymer system held static throughout the run. These rigid simulations were run for 2,000,000 MC steps with the final one-third of the data used to calculate equilibrium averages (**Figures S3 and S4**). The flexible method employed iterative MC and MD



(MCMD), where one iteration consisted of 2,000,000 MC steps followed by 2 ns of isothermal–isobaric MD with a 0.5 fs timestep to allow for system relaxation. All inserted gas molecules were intramolecularly fixed (i.e., no bending or stretching) but were allowed to rotate and translate during MD. The 0.5 fs timestep was used to account for this rigid adsorbate assumption as reported previously.³⁸ Each flexible isotherm was run for at least 5 cycles at each pressure point, but cycles were continued until they converged (**Figure S5** and **Table S2**). To achieve these flexible simulations, communication between LAMMPS and Cassandra was performed with the Python-based pysimm package (using an in-house modified distribution of version 1.1, both of which are open-source).^{71–75} The flexible method provides a more realistic system description of condensable gas uptake by allowing molecular rearrangement, but it is significantly more computationally expensive than the rigid method.

3.5 Uncertainty and Error Propagation

As CANAL-Me-Me₂F is amorphous, five different systems were generated independently using Polymatic. Uncertainties in “static” properties (i.e., properties that were directly calculated from the equilibrated polymer system, e.g., density) were determined as the sample standard deviation between the five replicates. Uncertainties in Monte Carlo simulations were determined as the sample standard deviation of the fluctuations within each replicate’s equilibrium value, followed by error propagation between the five replicates.⁷⁶

3.6 Gravimetric and Volumetric Sorption

Depending on the study, results may be reported gravimetrically (e.g., mmol g^{−1}) or volumetrically (e.g., cm³_{STP} cm^{−3}_{pol}) where conversion between the two is described as follows:

$$C = 22.414 \frac{\text{cm}^3_{\text{STP}}}{\text{mmol}} \cdot q \cdot \rho_{\text{pol}} \quad (10)$$

where C is the volumetric concentration (cm³_{STP} cm^{−3}_{pol}), q is the gravimetric loading (mmol g^{−1}), and ρ_{pol} is the polymer density (g cm^{−3}). Preference between the two forms is largely dependent on the material



form factor and the experimental techniques for measurements. For *in silico* studies, results have been reported using both methods.^{37,77}

While both methods are reasonable, challenges arise when attempting to compare computational results to experimental. Since the polymer density within the simulation may not match that of experiment, as has been previously shown by Abbott et al.³⁴ for PIM-1, the conversion between measurement styles can influence comparison between simulated and experimental results. To account for this density difference, the simulated volumetric results reported here are scaled by the ratio of experimental to simulated densities, effectively normalizing the results so that they are comparable regardless of measurement style reported. In other words, the ρ_{pol} used in the conversion is the experimental density, not the simulated density.

4. Experimental Methods

4.1 Density Measurements

CANAL-Me-Me₂F films were solution cast and subject to methanol treatment using the same procedure described in Lai et al.⁵ The density of the films was measured using a gravimetric approach, and the area was determined using a hand-traced polygon in ImageJ software (version 1.51k).⁷⁸ The thickness across the films was measured using a Mituyo (Kanagawa, Japan) micrometer, with an accuracy of $\pm 1.27 \mu\text{m}$.

4.2 Free Volume Distribution via Non-Local Density Functional Theory (NLDFT)

BET surface areas of the CANAL-Me-Me₂F polymers were measured with an N₂ probe at 77 K using a Micromeritics ASAP 2020 with the same procedure as described in Lai et al.⁵ Analysis of free volume distributions (3.6–20 Å) was performed using the non-local density functional theory (NLDFT) model for carbon slit pore geometry using the SAIEUS software, which implements the L-curve method for the regularization parameter, λ .⁷⁹



4.3 Experimental Gas Sorption Isotherm Measurements

Gas sorption isotherms for the CANAL-Me-Me₂F films were collected using an automated constant-volume pressure-decay system from Maxwell Robotics (Austin, TX) at 35 °C. A detailed protocol for these tests can be found in previous work by Mizrahi Rodriguez et al.⁸⁰

4.4 Thermal Expansion Coefficient via Dynamic Mechanical Analysis (DMA)

To understand the dimensional change in the CANAL-Me-Me₂F films during heating, the length of each film was continuously measured using a single screw film clamp test experiment on a TA Instruments (New Castle, DE) DMA Q850 using a heating (30 to 140 °C) and cooling procedure (140 to 30 °C) with a ramp rate of 5 °C min⁻¹.

4.5 Materials

Chloroform (HPLC grade) and methanol (ACS reagent grade) were purchased from Sigma Aldrich (St. Louis, MO). The following gases were purchased from Airgas (Radnor, PA): He (>99.999%), H₂ (>99.999%), N₂ (>99.999%), O₂ (>99.999%), CH₄ (>99.99%), H₂S (air certified standard mixture, 99.99%), C₃H₆ (>99.0%), and C₃H₈ (>99.0%). CANAL-Me-Me₂F polymer used for C₃H₈ and C₃H₆ sorption and density measurements was purchased from Osmoses (Cambridge, MA). CANAL-Me-Me₂F polymer used for H₂, O₂, N₂, and CH₄ sorption is the same polymer as previously studied by Lai et al.⁵

5. Results and Discussion

5.1 System Validation

The chosen molecular system parameters were validated via structural property alignment between simulated and experimental systems. To make this validation, bulk density, skeletal density, free volume distribution (FVD), and the static structure factor of the simulated system were determined.

Bulk density is defined as



$$\rho_{bulk} = \frac{m}{V_{tot}} \quad (11)$$

where m is the system's total mass and V_{tot} is the system volume, including void space. Skeletal density, ρ_{skel} , is the density of the system, removing void volume, V_{void} :

$$\rho_{skel} = \frac{m}{V_{skel}} = \frac{m}{V_{tot} - V_{void}} \quad (12)$$

Skeletal densities were calculated using PoreBlazer (version 4.0)⁸¹ with a helium probe ($d = 2.60 \text{ \AA}$) and mapping via the Connolly surface algorithm, as done previously by Abbot et al. for PIM-1.^{36,55,82}

The experimental bulk density at room temperature of $0.96 \pm 0.02 \text{ g cm}^{-3}$ led to differences of 17% and 1% compared to the bulk densities of the UA and AA frameworks at $35 \text{ }^{\circ}\text{C}$, respectively. Abbot et al.³⁶ reported simulated bulk densities for UA frameworks consistently lower than experimental bulk densities for multiple polymers (PS, PMMA, PET, PC, PEI, PIM-1) when polymerized with Polymatic, hypothetically due to difficulty in comparing geometrically- and experimentally-derived densities, especially for high free volume polymers, where differences are likely amplified.

The simulated bulk density of the polymer decreases with increasing temperature for both the UA and AA frameworks as shown in **Figure 1**. Interestingly, the slopes of the density versus pressure plots for both the UA and AA frameworks are remarkably similar at $(-2.2 \pm 0.2) \cdot 10^{-4} \text{ g cm}^{-3} \text{ K}^{-1}$ and $(-2.3 \pm 0.2) \cdot 10^{-4} \text{ g cm}^{-3} \text{ K}^{-1}$, respectively for bulk density. Free volume theory predicts an increase in free volume should increase the volumetric thermal expansion coefficient, α_V , defined as⁸³:

$$\alpha_V = \frac{1}{V} \left(\frac{\partial V}{\partial T} \right)_P = -\frac{1}{\rho} \left(\frac{\partial \rho}{\partial T} \right)_P \approx -\frac{1}{\rho_0} \frac{\Delta \rho}{\Delta T} \quad (13)$$

where the approximation is valid for $\Delta \rho / \rho_0 \ll 1$ (Equations S2–S5). However, we hypothesize that our findings are due to both the UA and AA frameworks attempting to simulate the same underlying physical mechanisms. In other words, even though the frameworks' respective geometries create different equilibrium packing, the effect of temperature remains consistent across both frameworks. This hypothesis is further supported by noting that both AA^{84–86} and UA^{86–89} models are frequently employed to explore the



thermal behavior of amorphous polymers in both their rubbery and glassy regimes. The “macroscopic”⁹⁰ nature of examining density as a function of temperature may obfuscate any significant temperature-dependent differences that arise due to free volume discrepancies between UA and AA models, which may be occurring on a more microscopic scale. The data is also represented as the change in fractional free volume (FFV) with temperature in **Figure S8**.

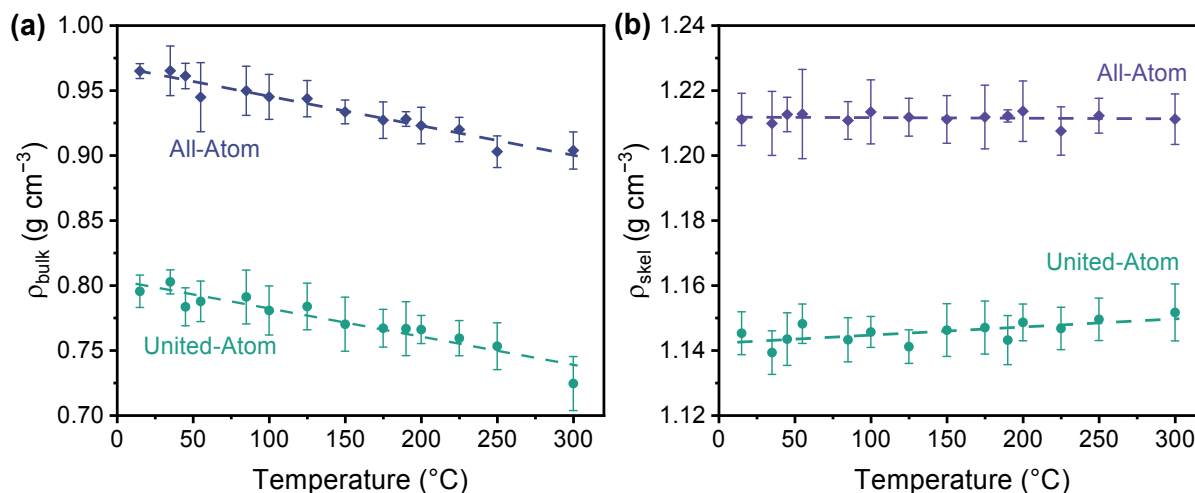


Figure 1. Temperature versus (a) bulk and (b) skeletal densities of simulated CANAL-Me-Me₂F for all-atom (AA) and united-atom (UA) frameworks. Dashed lines show linear regressions. Error bars represent uncertainty as the standard deviation over five independent CANAL-Me-Me₂F systems.

The experimental volumetric thermal expansion coefficient was determined from the linear thermal expansion coefficient (α_L) and, assuming isotropic expansion, calculated as⁹¹:

$$\alpha_V = 3\alpha_L \quad (14)$$

The α_V for both simulated and experimental systems is shown in **Table 1**. Two temperature ranges were selected for the simulated systems: one range that better aligns with the experimental data, and a second broader range to provide a value with reduced error by increasing the number of datapoints used. Both experimental and simulated results fall within the same order of magnitude and error. As one might expect based on their similar temperature dependence, the UA and AA systems have similar expansion coefficients. The experimental DMA expansion data is shown in Section S2.1. While the bulk density



changes with temperature, the skeletal density is nearly constant within uncertainty with temperature (skeletal density linear regressions: $(2.5 \pm 0.8) \cdot 10^{-5} \text{ g cm}^{-3} \text{ K}^{-1}$ and $(-2 \pm 5) \cdot 10^{-6} \text{ g cm}^{-3} \text{ K}^{-1}$, respectively, for UA and AA systems). This phenomenon indicates that the increase in temperature is increasing the void space between polymer chains with limited effect on the skeletal structure.

Table 1. Volumetric thermal expansion coefficients (α_V) for simulated and experimental systems compared to select glassy polymers.

System	Polymer	$\alpha_V (10^4 \cdot \text{K}^{-1})$	Temperature Range ($^{\circ}\text{C}$)
United-Atom	CANAL-Me-Me ₂ F	2.2 ± 0.8	35–150
		2.7 ± 0.3	15–300
All-Atom	CANAL-Me-Me ₂ F	2.1 ± 0.8	35–150
		2.4 ± 0.2	15–300
Experimental	CANAL-Me-Me ₂ F	$1.0\text{--}2.2^a$	35–139
Experimental ⁹²	polystyrene	$1.8\text{--}2.4$	$< T_g$
Experimental ⁹²	poly(methyl methacrylate)	2.1	$< T_g$
Experimental ⁹³	cellulose acetate	3.3^b	$< T_g$
Experimental ⁹⁴	PIM-1	2.1	30–110

^aAs further explained in Section S2.1, the experimental α_V was found using a polynomial fit, creating a non-constant value.

^bReference provided α_V , thus, Equation 14 was not applied.

To better understand the polymer microstructure, the FVD was calculated using PoreBlazer, defined as the negative derivative of the cumulative free volume, V , with respect to the probe diameter, D :

$$FVD \equiv -\frac{dV(D)}{dD} \quad (15)$$

The FVD is also commonly referred to as the pore size distribution (PSD), including within PoreBlazer, however, FVD is used here to distinguish the micropores within these polymers from more classically defined porous materials. As the location of atoms is required, this geometric FVD method is only applicable to simulated systems. Experimental FVD determination relies on indirect methods such as NLDFT^{40,95,96} or positron annihilation lifetime spectroscopy (PALS).^{7,97,98} **Figure 2a** compares experimentally determined FVD via NLDFT to geometric FVD using a helium probe ($d = 2.60 \text{ \AA}$)⁸² which reveals significant differences between the two methods. To ensure differences between probe size and/or temperature were not significantly altering the geometric FVD, a nitrogen ($d = 3.64 \text{ \AA}$)⁸² probe was also considered for simulations at 77 K and 308 K (**Figure S7**). These results are in agreement with a previous



study by Kupgan et al.,⁴⁰ which showed NLDFT to systematically overpredict free volume elements (FVEs) for amorphous polymers, including PIM-1. When considering the impressive ability for microporous organic polymers, including CANAL-Me-Me₂F, to selectively separate gases below diameters of 4 Å, it is further evidence of FVD overprediction using NLDFT methods, as these methods predict all pores to be larger than 4 Å.^{5,20}

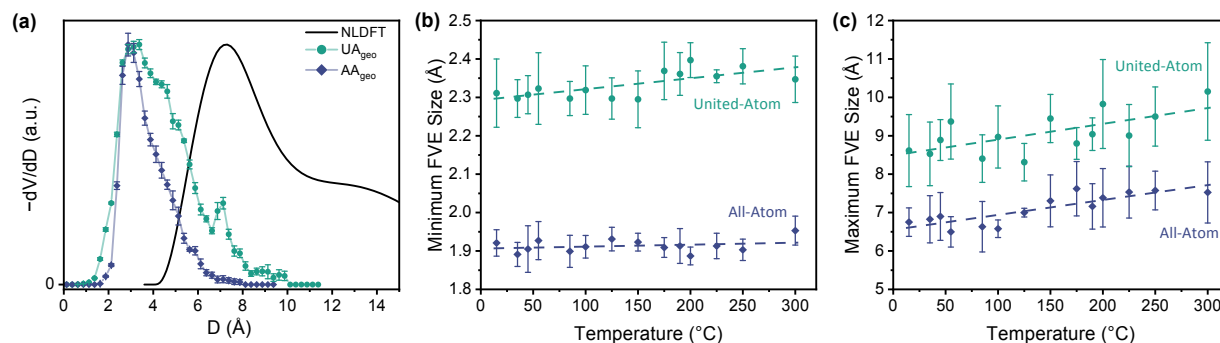


Figure 2. (a) Free volume distributions (FVDs) of CANAL-Me-Me₂F from non-local density functional theory (NLDFT) via experimental N₂ sorption measurements at 77 K as well as simulated geometric determination from united-atom (UA) and all-atom (AA) simulations at 35 °C using a helium probe. Solid lines are meant to guide the eyes. Data are normalized to their maximum ordinate value. (b) Minimum and (c) maximum FVEs present in the UA and AA CANAL-Me-Me₂F frameworks across a temperature range of 15–300 °C. Dashed lines show linear regressions.

Figure 2b and **c** detail the minimum and maximum pore sizes present, taken as the values at which 99% and 1% of the cumulative free volume was accessible, respectively, over a 15–300 °C temperature range. The AA framework shows a narrower FVD than the UA framework across all temperatures. The FVD is seen to broaden with increasing temperature—largely due to the increase in the maximum FVE size, which increases an order of magnitude faster than the minimum FVE size. These results agree with the density decreasing as a function of temperature, as free volume elements may increase in size as the polymer expands. The more uniform minimum FVE size with increasing temperature suggests that even though the



average FVE size may increase, there remain stochastically fluctuating pockets that maintain gas sieving capabilities even at high temperatures.

Crystallographic data was computed using the Interactive Structure Analysis of Amorphous and Crystalline Systems (ISAACS) program (version 2.10).⁹⁹ The static structure factor, $S(q)$, was used to compare against experimental wide-angle X-ray scattering (WAXS) data from Lai et al.⁵ The simulated scattering data reasonably follows the experimentally gathered data with a broad amorphous halo around 1.0 \AA^{-1} as shown in **Figure 3**. The d-spacing for the amorphous halo of the experimental results is 7.1 \AA , while that of the UA and AA results are 6.6 \AA and 6.5 \AA , respectively. For the experimental result, the increase in intensity as q goes to zero is not visible in the simulated static structure factor and is attributed to experimental error as the regime around and below 0.3 \AA^{-1} is better suited for small-angle X-ray scattering (SAXS).¹⁰⁰

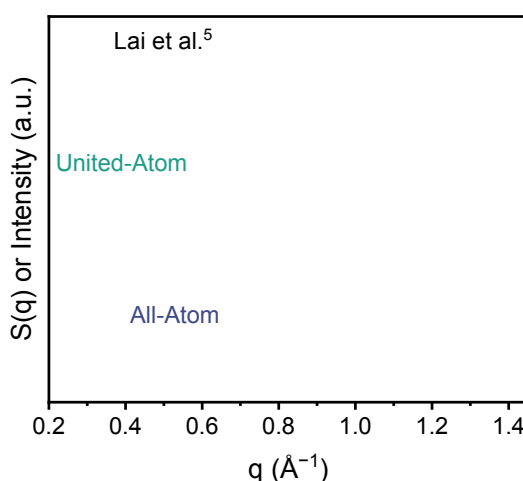


Figure 3. Experimental wide-angle X-ray scattering (WAXS) data (solid line) from Lai et al.⁵ compared with simulated static structure factors of all-atom (dotted line) and united-atom (dashed line) CANAL-Me-Me₂F systems. Error bands represent the sample standard deviation from five replicate polymer systems. Data are normalized to their maximum ordinate value in the range $0.9\text{--}1.1 \text{ \AA}^{-1}$.

5.2 Small-Gas Sorption Isotherms

This study focuses primarily on H₂S, C₃H₆, and C₃H₈, which are plasticizing gases. When compared to smaller gases, such as H₂ and N₂, these larger gases create complexities with modeling, such as the need for



additional force field parameters and iterated MCMD. To better understand limitations specific to the polymer model itself, sorption isotherms for fixed-framework UA models of H₂, N₂, O₂, and CH₄ were simulated at 35 °C and compared to experimentally obtained sorption isotherms, shown in **Figure 4**. Because these smaller gases do not cause detectable polymer plasticization, flexible frameworks do not provide increased convergence with experimental results, as shown explicitly in **Figure 4a** and **d** for H₂ and CH₄, respectively.

The simulated systems show quantitative agreement with experimental results. Specifically, results for H₂, N₂, and O₂ fall within error of experimental values, while results for CH₄ show slight under- or overprediction depending on whether an MC or MCMD procedure was applied. The usage of a flexible framework increases the sorbed concentration of a gas when compared to the rigid framework, as polymer rearrangement within the flexible framework allows gas molecules to settle in previously inaccessible locations. These results indicate the ability for the CANAL-Me-Me₂F model to quantitatively model sorption using GCMC for non-plasticizing gases and give credence to the relevance of the chosen forcefield parameters. The ability to model experimental isotherms agrees with previous studies that have found GCMC to be a valuable tool for predicting sorption of non-plasticizing gases in polyimides, porous aromatic frameworks, and PIMs.^{35,101,102}



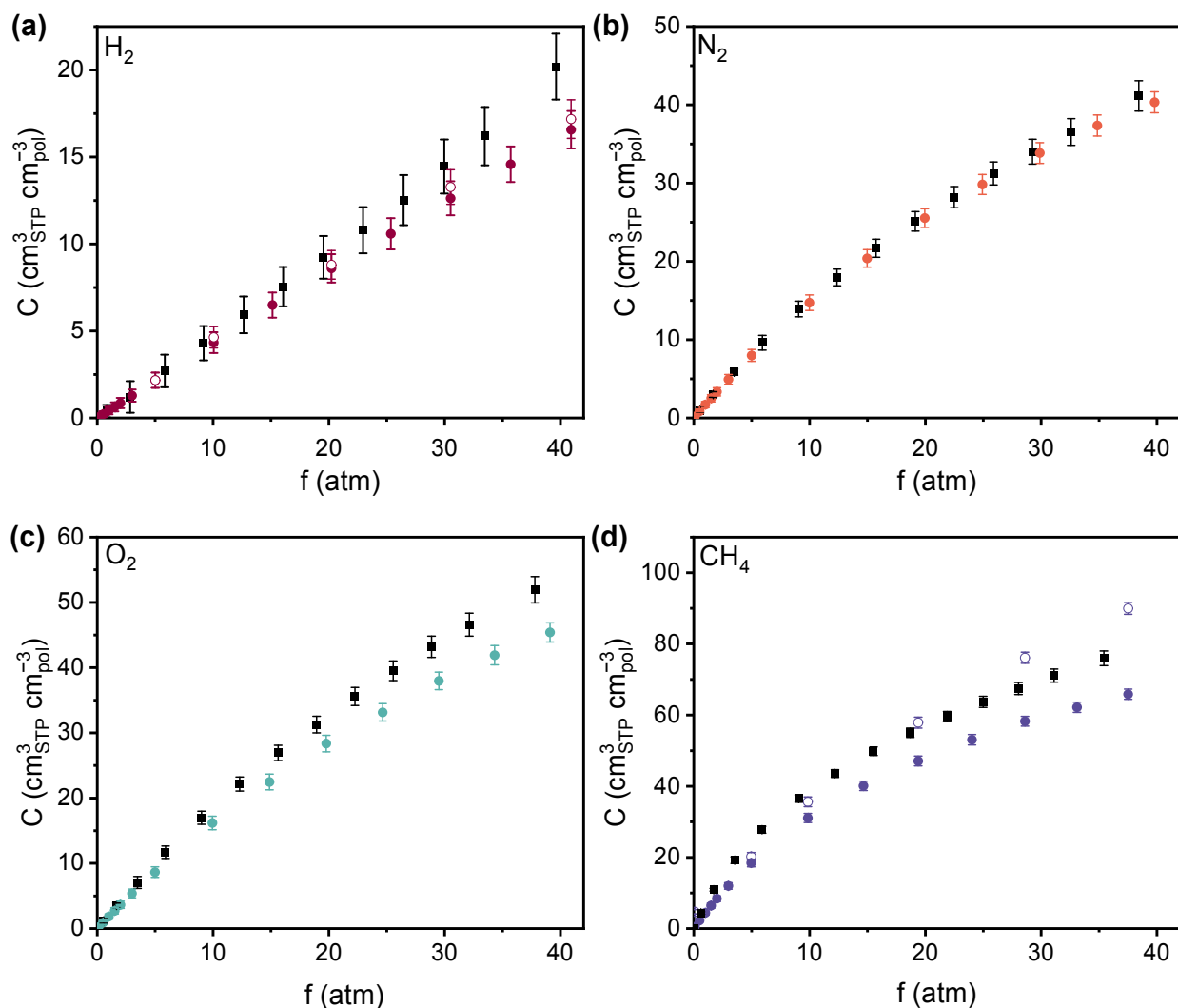


Figure 4. Comparisons of united-atom simulations and experimental (black squares) isotherms in CANAL-Me-Me₂F for (a) H₂, (b) N₂, (c) O₂, and (d) CH₄, all at 35 °C. Rigid (filled datapoints) and flexible (unfilled datapoints) isotherms were computed for H₂ and CH₄ while only rigid isotherms were computed for N₂ and O₂. Fugacity was calculated via a second-order Virial expansion.¹⁰³

5.3 Plasticizing Gas Sorption Isotherms

For plasticizing gases (e.g., CO₂, H₂S, C₃H₆, and C₃H₈), the effects of fixed versus flexible framework were significant, as exemplified in **Figure 5**. For CO₂, the flexible framework overpredicted yet showed qualitative agreement with experimental results at fugacities below 20 atm before strongly diverging.



Interestingly, for CO₂, the flexible framework performed worse than the fixed framework. The flexible framework model for H₂S underpredicted yet qualitatively aligned with the experimental H₂S isotherm. For the larger C₃H₆ and C₃H₈ hydrocarbons, quantitative agreement with experimental isotherms is demonstrated at low to moderate fugacities (<3 atm), indicating the applicability of this flexible framework. These comparisons with experimental results highlight how the polar molecules (CO₂ and H₂S) show poorer alignment with experimental results than the hydrocarbons. This result could be due to the additional force field complexities that arise for interparticle interactions when significant polarity is present, amplifying the relative simplicity of force fields compared to actual molecular electronic behavior. Therefore, even for plasticizing gases, it is advisable to compare both fixed and flexible frameworks to determine which is best for specific cases.



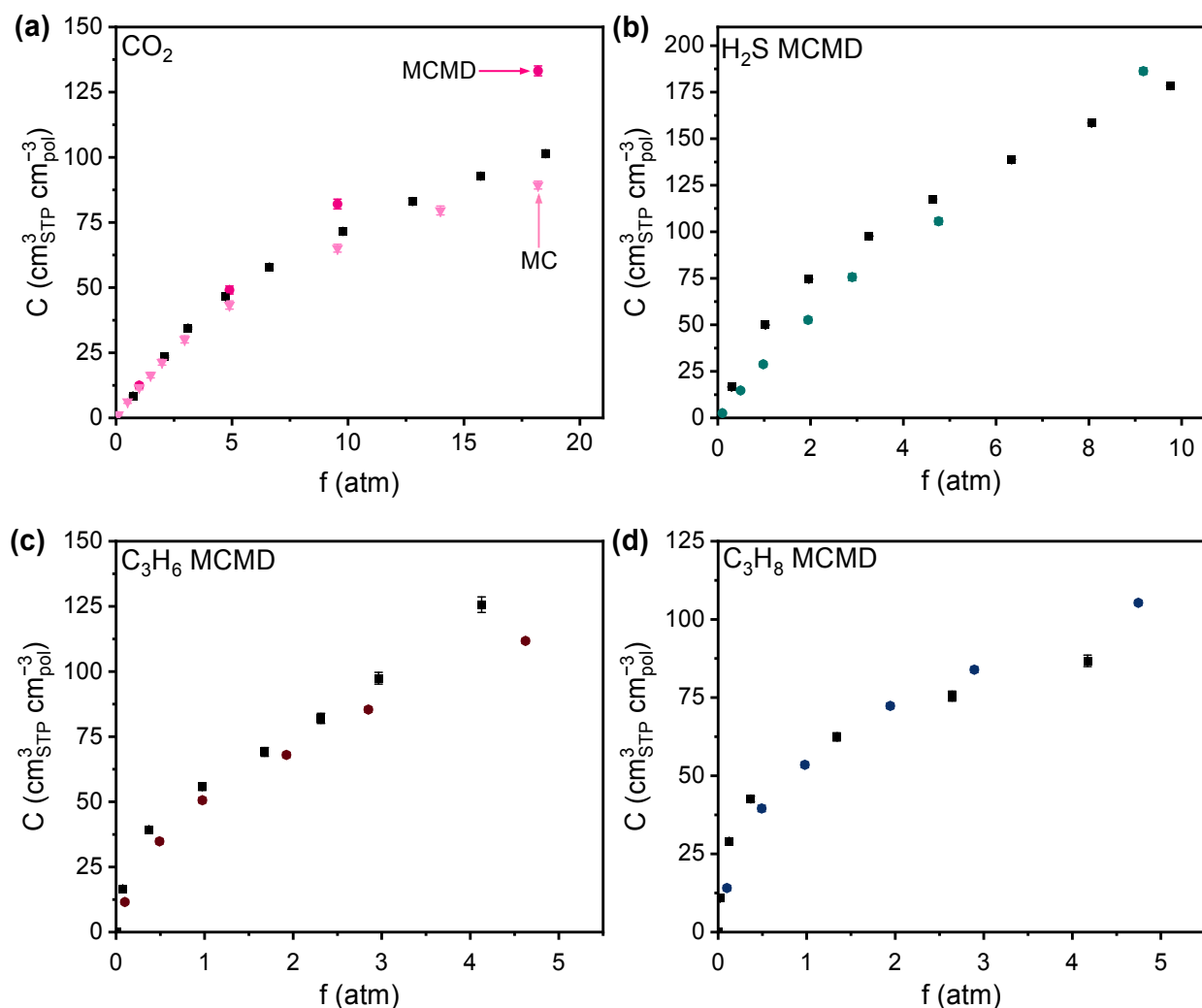


Figure 5. Comparison of flexible framework united-atom simulations and experimental isotherms in CANAL-Me-Me₂F at 35 °C for (a) CO₂, (b) H₂S, (c) C₃H₆, and (d) C₃H₈. Experimental results are shown with black squares while flexible framework (MCMD) simulations are shown with colored circles. Fixed framework united-atom simulations are shown for CO₂ in (a) as triangles. Fugacity was determined for CO₂, C₃H₆ and C₃H₈ via a second-order Virial expansion and for H₂S with the Peng-Robinson equation of state.^{103–105} The experimental H₂S isotherm has previously been reported in Yeo et al.²⁰

Previous studies that have examined CO₂ sorption in PIM-1 using the iterative MCMD approach have reported both under- and overfitting compared to experimental results.^{38,106} The broad range of CO₂ sorption isotherms in PIM-1 is indicative of the fact that slight changes in reaction conditions, post-treatment, and



testing methods can significantly alter the results.¹⁰⁷ Compounding these challenges is the issue that simulated “synthesis,” relaxation, and sorption measurements are unable to be performed as one would do experimentally. Thus, we emphasize that divergence from experimental results is not unexpected given these limitations and experimental scatter.¹⁰⁸

5.4 Dual-Mode Sorption Model

A LFER-constrained DMS model has previously been applied to CANALs and H₂S sorption in glassy polymers.^{23,109} Here, we extend those H₂S results reported at 35 °C to 35–190 °C. Sorption isotherms and their corresponding DMS fits are shown in **Figure 6** with DMS parameters tabulated in **Table 2**. As the effect of Langmuir sorption decreases with increasing temperature due to the deactivation of surface modes and the exothermic nature of Langmuir sorption, the sorption isotherms become more linear with increasing temperature. Details on the DMS fitting procedure including initial guesses and parameter bounds (**Tables S4–5**) are available in the SI.

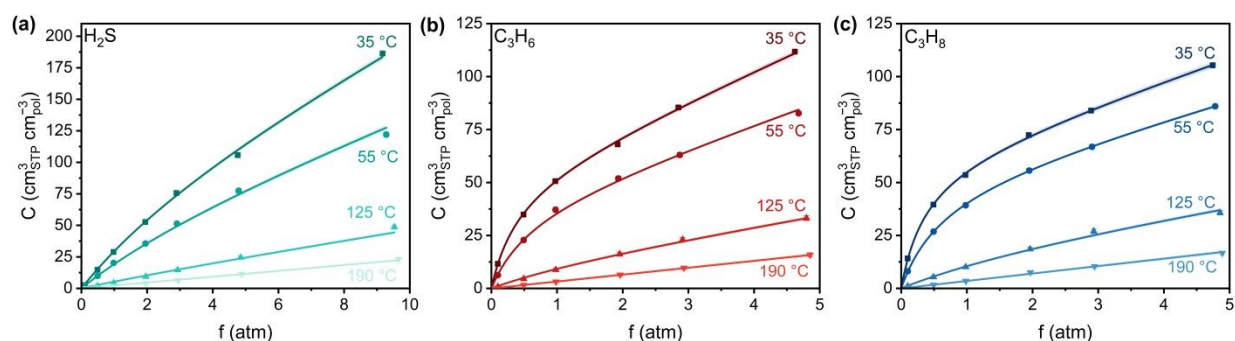


Figure 6. Simulated MCMD sorption isotherms and corresponding dual-mode sorption (DMS) model fits for (a) H₂S, (b) C₃H₆, and (c) C₃H₈ at temperatures of 35 °C, 55 °C, 125 °C, and 190 °C. DMS fits were restricted via linear-free energy relationships (LFERs) and van't Hoff constraints as implemented by Wu et al.³⁰ Uncertainties in DMS parameters were estimated from the inverse of the Hessian of χ^2 at the optimum, followed by standard error propagation to determine uncertainty in concentration.⁷⁶



Table 2. Dual-mode sorption parameters for CANAL-Me-Me₂F, fit using an LFER-constrained model.³⁰

Gas	Temperature (°C)	k_D (cm ³ _{STP} cm ⁻³ _{pol} atm ⁻¹)	C'_H (cm ³ _{STP} cm ⁻³ _{pol})	b (atm ⁻¹)
H ₂ S	35	13.7 ± 0.2	87 ± 3	0.223 ± 0.002
	55	9.9 ± 0.1	54 ± 2	0.210 ± 0.005
	125	4.12 ± 0.03	8 ± 2	0.18 ± 0.02
	190	2.32 ± 0.01	0.0 ± 0.5	0.16 ± 0.03
C ₃ H ₆	35	13.5 ± 0.2	53 ± 1	2.40 ± 0.04
	55	10.4 ± 0.1	40.5 ± 0.4	1.60 ± 0.01
	125	5.2 ± 0.1	12 ± 1	0.54 ± 0.03
	190	3.5 ± 0.1	0 ± 1	0.26 ± 0.02
C ₃ H ₈	35	10.2 ± 0.2	61 ± 1	2.64 ± 0.05
	55	8.4 ± 0.1	52 ± 1	1.58 ± 0.01
	125	5.0 ± 0.1	20 ± 1	0.39 ± 0.01
	190	3.5 ± 0.1	0 ± 1	0.16 ± 0.01

In the optimization, no functional form was fit to the Langmuir capacity constant, C'_H , as it has previously been fit to both linear¹¹⁰ and van't Hoff temperature dependent models,³³ as shown in Equations 16 and 17, respectively:

$$C'_{H,j} = \alpha_{1,j} + a_{2,j}T \quad (16)$$

$$C'_{H,j} = \beta_{1,j} \exp\left(-\frac{\beta_{2,j}}{RT}\right) \quad (17)$$

where $\alpha_{i,j}$ and $\beta_{i,j}$ are fitting parameters for gas j . The DMS results presented here allow for an analysis of the C'_H parameter from the LFER-constrained DMS model across a large range of temperatures. As shown in **Figure 7**, both models show similar goodness-of-fit. The log-modified mean absolute percentage error (MAPE)¹¹¹ for each model is shown in **Table 3**, indicating that the more applicable model in a given scenario is dependent on the specified gas and temperature. However, when extrapolating towards $C'_H = 0$ to approximate where Langmuir sorption is no longer present, the proposed van't Hoff relationship significantly overpredicts the corresponding temperatures compared to the linear fit. The linear fits predict there to be a loss of Langmuir sorption between 132–167 °C, as is reflected in the sorption isotherms of **Figure 6** where the sorption isotherms at 190 °C exhibit negligible Langmuir contribution. As the van't Hoff relationship does not allow for determination at $C'_H = 0$, results are reported for $C'_H = 1$. This van't Hoff fit does not predict loss of Langmuir sorption until between 262–1279 °C. This broad range illustrates



the limitations of using phenomenological models for material property predictions and corroborates conclusions by Koros and Paul¹¹⁰ and Koros et al.³³ who determined that while the van't Hoff fit is “convenient,” it lacks theoretical justification. The linear fit, they argued, can be better related to the free volume within the polymer below its glass transition temperature and subsequent vanishing at the glass transition temperature. A comprehensive study of Xe sorption and ¹²⁹Xe NMR using poly(*p*-phenylene oxide) supported the observation that a linear extrapolation of C'_H to zero corroborates well with the location of the T_g , where C'_H is expected to become negligible.¹¹²

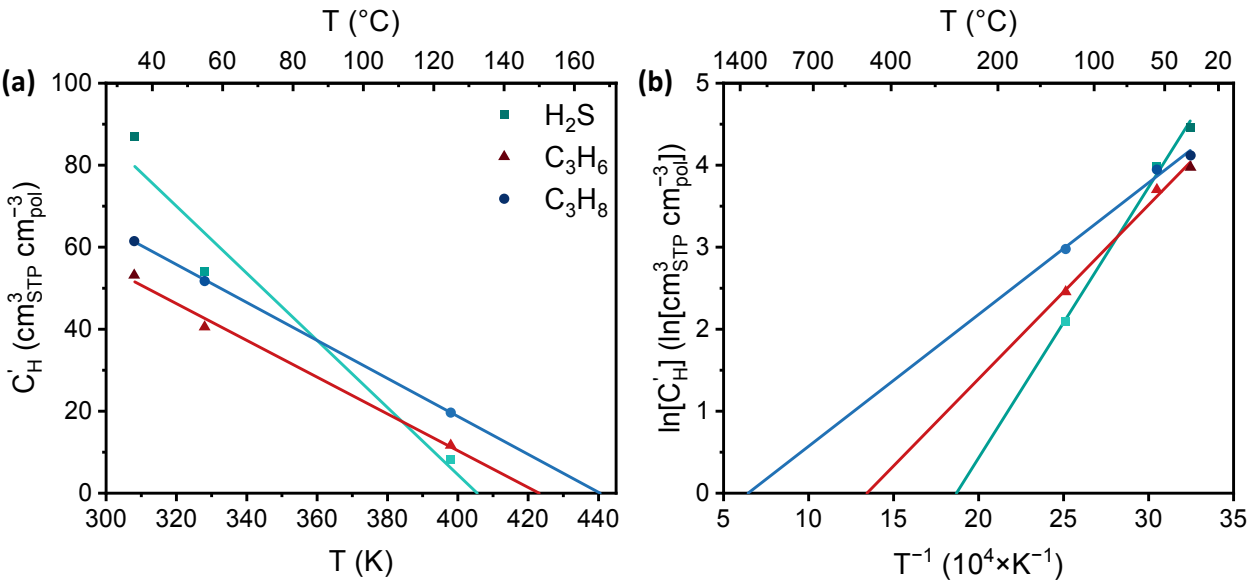


Figure 7. (a) Linear and (b) van't Hoff fits for C'_H versus temperature and inverse temperature, respectively, for H_2S (green squares), C_3H_6 (red triangles), and C_3H_8 (blue circles). Fits are shown extrapolated to (a) $C'_H = 0$ and (b) $C'_H = 1$.

Table 3. Log-modified mean absolute percentage error (MAPE) and extrapolated temperature where $C'_H = 0$ for linear and $C'_H = 1$ for van't Hoff fits of C'_H versus temperature and inverse temperature, respectively.

Gas	Linear Fit		Van't Hoff Fit	
	Modified MAPE (%)	$T_{C'_H=0}$ (°C)	Modified MAPE (%)	$T_{C'_H=1}$ (°C)
H_2S	3.0	132	7.8	262
C_3H_6	2.5	150	1.7	471
C_3H_8	2.4	167	0.2	1279

5.5 Sorption Energetics

To better understand polymer–gas affinity between CANAL-Me-Me₂F and C₃H₆, C₃H₈, and H₂S, as well as to understand how these results differ from the archetypal microporous polymer, PIM-1, the thermodynamics of sorption were analyzed via the DMS model. The same LFER-constrained model as detailed above for CANAL-Me-Me₂F was used for PIM-1. The DMS parameters for H₂S in PIM-1 were computed from the isotherms of Dean et al.²³ The DMS parameters for C₃H₆ and C₃H₈ in PIM-1 were computed from the isotherms of Li et al.¹¹³ These parameters are reported in **Table S7**. We note that when using an unconstrained DMS optimization, sorption energetics in PIM-1 can lead to significantly different values and trends (**Table S9**), thus, efforts to constrain parameters to physically-relevant trends are vital to more reliable structure–property relationships.

Langmuir sorption, as shown in **Figure 8a** and **Table S6**, is responsible for over 55% of infinite dilution sorption at 35 °C for H₂S and over 90% for the two hydrocarbons. By 125 °C, however, these values decrease to between 25% and 65%, indicating the stronger temperature dependence of Langmuir sorption compared to Henry sorption. As shown in **Figure 8b**, the sorption coefficient at infinite dilution, S_{∞} , of H₂S in PIM-1 has a larger contribution from the Langmuir mode than CANAL-Me-Me₂F. This result correlates with the lower plasticization pressure of CANALs.²⁰ The significantly lower S_{∞} for H₂S in CANAL-Me-Me₂F was expected due to the degree of linearity exhibited in the isotherms shown in **Figure 6a**.



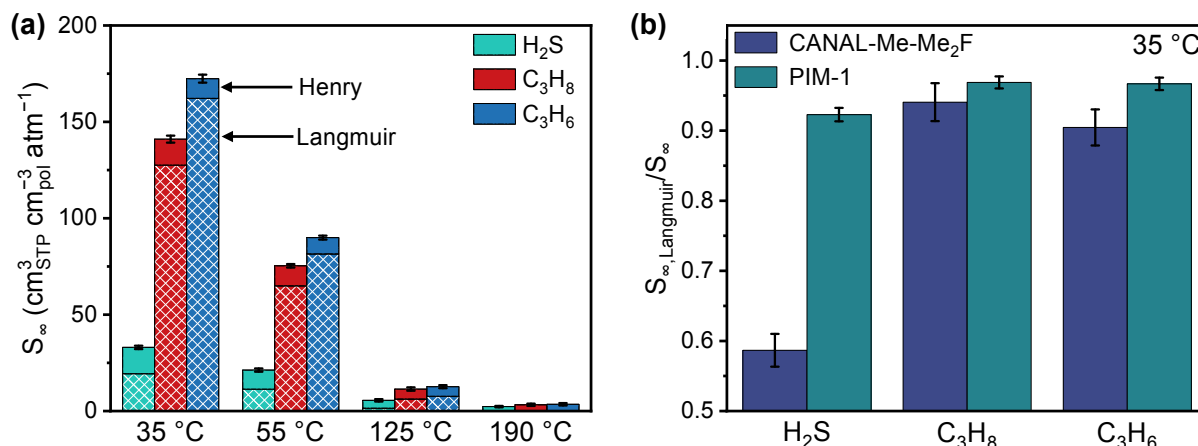


Figure 8. (a) Sorption coefficient at infinite dilution (S_{∞}) for H_2S , C_3H_6 , and C_3H_8 in CANAL-Me-Me₂F at temperatures of 35 °C, 55 °C, 125 °C, and 190 °C. Uncertainty is propagated from uncertainty in the DMS parameters and shown as the combined uncertainty of both Langmuir and Henry modes. (b) Percent contribution of S_{∞} from the Langmuir mode for CANAL-Me-Me₂F and PIM-1, compared for H_2S , C_3H_6 and C_3H_8 at 35 °C. PIM-1 parameters were fit using previously published isotherms.^{23,113}

As detailed explicitly in **Table 4**, the trends in heats of sorption differ between CANAL-Me-Me₂F and PIM-1. Analysis of the energetics of infinite dilution sorption for the two hydrocarbons showed that in PIM-1, C_3H_6 was significantly more exothermic than C_3H_8 ($\Delta H_{S,\infty,\text{C}_3\text{H}_6} - \Delta H_{S,\infty,\text{C}_3\text{H}_8} \approx -20 \text{ kJ mol}^{-1}$) while in CANAL-Me-Me₂F, the two terms were nearly within uncertainty of each other ($\approx 1 \text{ kJ mol}^{-1}$). These differences in energetics between the two hydrocarbons are most significantly due to partitioning within the Langmuir regime, as differences in ΔH_D between C_3H_6 and C_3H_8 were within 3 kJ mol^{-1} for both polymers.

Table 4. Heats of infinite dilution ($\Delta H_{S,\infty}$), Henry (ΔH_D), and Langmuir sorption (ΔH_b) for H_2S , C_3H_6 , and C_3H_8 in CANAL-Me-Me₂F and PIM-1.^{23,113}

Polymer	Gas	$\Delta H_{S,\infty} (\text{kJ mol}^{-1})$	$\Delta H_D (\text{kJ mol}^{-1})$	$\Delta H_b (\text{kJ mol}^{-1})$
CANAL-Me-Me ₂ F	H_2S	-20.5 ± 0.2	-13.6 ± 0.1	-2 ± 1
	C_3H_6	-29.0 ± 0.3	-10.9 ± 0.3	-17 ± 1
	C_3H_8	-30.0 ± 0.3	-8.2 ± 0.4	-22 ± 1
PIM-1	H_2S	-27.2 ± 0.2	-17.0 ± 0.3	-23.2 ± 0.2
	C_3H_6	-38 ± 1	-22.1 ± 0.1	-33.5 ± 0.3
	C_3H_8	-18 ± 1	-22 ± 1	-12 ± 1



The differences seen in the energetics of surface sorption of C_3H_6 and C_3H_8 between CANAL-Me-Me₂F and PIM-1 are hypothesized to be due to the heteroatoms within PIM-1 that are not present in CANAL-Me-Me₂F. Propylene is more polarizable than propane, leading to potentially stronger interactions between the nitrile functionality in PIM-1 and the π -bond in propylene.¹¹⁴ While no other studies on propylene sorption in CANALs have been performed, this effect can be likened to how increased side group polarity in PIM-1 (e.g., conversion of nitrile groups to primary amines), increases the sorption selectivity of propylene over propane.¹¹⁵ To further support the polarizability hypothesis, sorption simulations as described previously were conducted on a hypothetical CANAL-Me-Me₂F-like polymer with two methyl groups per repeat unit substituted for nitrile groups (CANAL-Me-Me₂F-CN), as shown in **Figure 9**. As shown in **Figure 10**, the Langmuir energetics of propylene were made more exothermic relative to propane while the Henry energetics remained similar. Details on the computational modeling of CANAL-Me-Me₂F-CN are available in Section S1.5 and DMS parameters are available in **Table S8**.

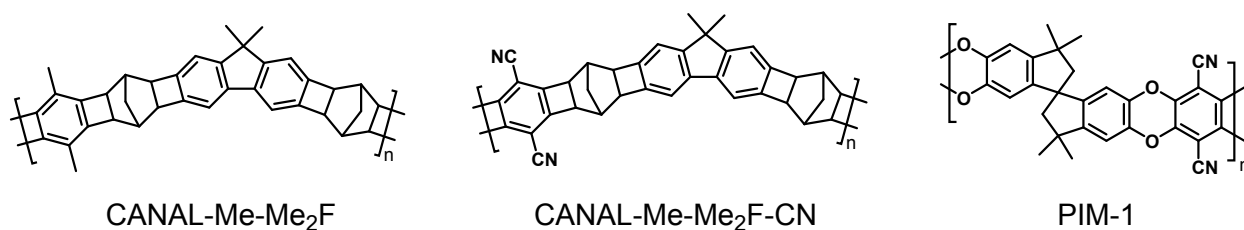


Figure 9. Structures of CANAL-Me-Me₂F, CANAL-Me-Me₂F-CN, and PIM-1. Note that the CANAL-Me-Me₂F-CN structure is hypothetical.



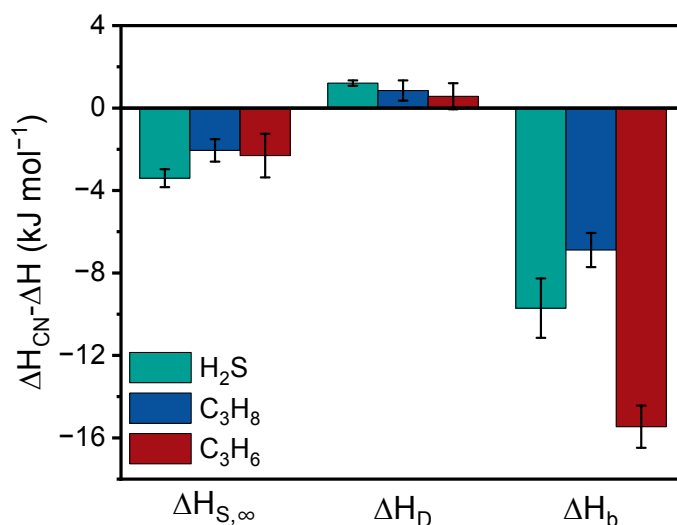


Figure 10. Difference in heats of sorption between CANAL-Me-Me₂F-CN (ΔH_{CN}) and CANAL-Me-Me₂F (ΔH) for infinite dilution, Henry, and Langmuir sorption from constrained DMS optimization routines.

Similar to the previously described differences in Langmuir sorption of C₃H₆ in CANAL-Me-Me₂F and PIM-1, H₂S, as a polar molecule, demonstrates more exothermic Langmuir sorption in PIM-1 ($\Delta H_b \approx -23$ kJ mol⁻¹) than in CANAL-Me-Me₂F (≈ -2 kJ mol⁻¹). As also shown in **Figure 10**, the Langmuir energetics of H₂S are more exothermic in CANAL-Me-Me₂F-CN than in CANAL-Me-Me₂F. Due to overlapping uncertainties between these energetic differences in H₂S and non-polar C₃H₈, however, these results are less conclusive than those of C₃H₆ described above.

Interestingly, ΔH_D values for all three gases in CANAL-Me-Me₂F are less exothermic than those obtained for the same gases in PIM-1. This result aligns with a previous finding that differences in sorption in the Henry's mode were strongly influenced by polymer backbone and less so on specific functionality.²³ In further agreement is that ΔH_D values between CANAL-Me-Me₂F and CANAL-Me-Me₂F-CN are within uncertainties of each other.

5.6 Mixed-Gas Sorption

To investigate the ability for CANAL-Me-Me₂F to perform the industrially relevant propylene/propane separation, the mixed-gas DMS model was applied. A 70/30 molar ratio of propylene/propane was chosen



as a balance between typical hydrocarbon stream composition from catalytic cracking (>80 mol% propylene) and from propane dehydrogenation (50 mol% propylene).^{116,117}

The effect of the mixed-gas DMS model on the sorption isotherms of C_3H_6 and C_3H_8 at 35 °C is shown in **Figure 11a**, yielding the characteristic decrease in Langmuir capacity with unchanged sorption effects of the Henry mode, as expected from the mixed-gas model formulation. The mixed-gas selectivities in CANAL-Me-Me₂F ($\alpha_{C_3H_6/C_3H_8}^S = S_{C_3H_6}/S_{C_3H_8}$) are shown in **Figure 11b**. Due to significant uncertainties in the selectivities, the effect of increasing temperature on selectivity from 35 °C to 190 °C cannot be definitively stated.

Comparison of the propylene/propane sorption selectivity between CANAL-Me-Me₂F and PIM-1 at 35 °C is shown in **Figure 11c**. CANAL-Me-Me₂F has a sorption selectivity below one for the majority of the fugacity range studied, while PIM-1 has a sorption selectivity near one. As Langmuir sites become saturated with increasing fugacity, the potential surface sorption differences between the two polymers as examined previously decrease in importance, and the propylene/propane selectivities in CANAL-Me-Me₂F and PIM-1 trend towards each other.

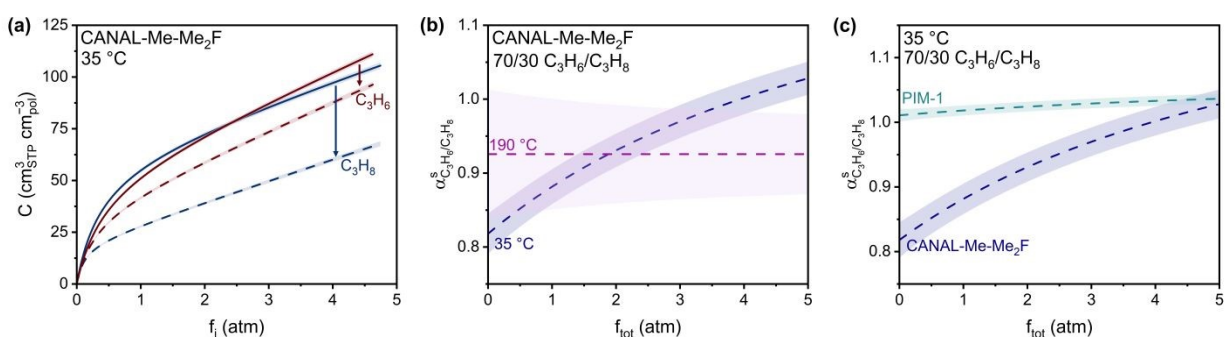


Figure 11. (a) Dual-mode sorption (DMS) isotherms for C_3H_6 and C_3H_8 in CANAL-Me-Me₂F for pure-gas (solid lines) and mixed-gas (dashed lines) for a 70/30 molar mixture of C_3H_6/C_3H_8 at 35 °C versus the fugacity of each component. DMS fits were restricted via linear-free energy relationships (LFERs) as implemented by Wu et al.³⁰ (b) Mixed-gas sorption selectivity of a 70/30 molar mixture of C_3H_6/C_3H_8 in CANAL-Me-Me₂F at 35 °C and 190 °C versus the combined fugacity of both penetrants. (c) Mixed-gas sorption selectivity of a 70/30 molar mixture of C_3H_6/C_3H_8 in CANAL-Me-Me₂F and PIM-1 at 35 °C versus



the combined fugacity of both penetrants. Data for CANAL-Me-Me₂F is from simulated MCMD isotherms. Data for PIM-1 is from the recomputed isotherms of Li et al.¹¹³

5. Conclusions

This study establishes an atomistic computational framework for CANAL polymers, which was validated against experimental data including density, free volume distribution (FVD), wide-angle X-ray scattering (WAXS), and sorption isotherms. Furthermore, a significant focus was placed on simulating the sorption and corresponding energetics of H₂S, C₃H₆, and C₃H₈, which are difficult to evaluate experimentally. While non-plasticizing gases were quantitatively modeled via GCMC, highly condensable gases—particularly the C₃H₆ and C₃H₈ hydrocarbons—required an iterative MCMD approach. These results support the use of MCMD simulations as a predictive tool, especially for time-intensive sorption studies and those with hazardous gases. Application of the dual-mode sorption (DMS) model over a broad range of temperatures from 35 °C to 190 °C for H₂S, C₃H₆, and C₃H₈ within CANAL-Me-Me₂F revealed the significant characteristic Langmuir-mode contribution to sorption at lower temperatures and pressures. By 190 °C sorption isotherms were nearly linear and characterized by the Henry mode. The higher Langmuir affinities for the hydrocarbons relative to H₂S in the purely hydrocarbon CANAL emphasizes how sorption in the CANAL polymer is largely driven by van der Waals interactions. Langmuir energetics were more exothermic for H₂S and C₃H₆ in PIM-1 than in CANAL-Me-Me₂F, potentially due to specific gas–polymer interactions made feasible through the nitrile group present in PIM-1, which was supported by simulations of a hypothetical nitrile-functionalized CANAL-Me-Me₂F. Overall, this work advances the understanding of condensable gas sorption in high free volume heteroatom-free ladder polymers. The microstructural and multi-temperature sorption analyses performed within this study suggest that increasing size-sieving through CANAL backbone modification can be quantified via geometric FVDs, aromaticity can be leveraged to favor Langmuir sorption of polarizable penetrants, and temperature can be used to significantly modulate the contribution of Langmuir sorption within CANALs. By validating an atomistic



simulation system for CANAL-Me-Me₂F, we provide a foundation for extending computational studies to other CANAL polymers. When used in conjunction with experiments, these simulations enable a more complete characterization of sorption behavior and support the rational design of membrane materials for complex gas separations.

6. Acknowledgements

The authors thank Pablo A. Dean for helpful discussions on the DMS model optimization, Cassiano G. Aimoli for helpful discussions on molecular simulations, Francesco M. Benedetti for sorption experiments of H₂, N₂, O₂, CH₄, and CO₂, and Ashley M. Robinson and Yan Xia for helpful discussions on CANAL polymer synthesis. The authors acknowledge the MIT SuperCloud, the Lincoln Laboratory Supercomputing Center, and the MIT Office of Research Computing and Data for providing HPC resources that have contributed to the research results reported within this paper. This work was supported by the U.S. Department of Energy, Office of Science Basic Energy Sciences Separation Science Program under Award DE-SC0023252.



References

- (1) Sholl, D. S.; Lively, R. P. Seven chemical separations to change the world. *Nature* **2016**, *532* (7600), 435–437. <https://doi.org/10.1038/532435a>.
- (2) Wijmans, J. G.; Baker, R. W. The solution-diffusion model: A review. *J. Membr. Sci.* **1995**, *107* (1), 1–21. [https://doi.org/10.1016/0376-7388\(95\)00102-i](https://doi.org/10.1016/0376-7388(95)00102-i).
- (3) Low, Z.-X.; Budd, P. M.; McKeown, N. B.; Patterson, D. A. Gas permeation properties, physical aging, and its mitigation in high free volume glassy polymers. *Chem. Rev.* **2018**, *118* (12), 5871–5911. <https://doi.org/10.1021/acs.chemrev.7b00629>.
- (4) McDermott, A. G.; Budd, P. M.; McKeown, N. B.; Colina, C. M.; Runt, J. Physical aging of polymers of intrinsic microporosity: a SAXS/WAXS study. *J. Mater. Chem. A* **2014**, *2* (30), 11742–11752. <https://doi.org/10.1039/c4ta02165g>.
- (5) Lai, H. W. H.; Benedetti, F. M.; Ahn, J. M.; Robinson, A. M.; Wang, Y.; Pinnau, I.; Smith, Z. P.; Xia, Y. Hydrocarbon ladder polymers with ultrahigh permselectivity for membrane gas separations. *Science* **2022**, *375* (6587), 1390–1392. <https://doi.org/10.1126/science.abl7163>.
- (6) Park, H. B.; Kamcev, J.; Robeson, L. M.; Elimelech, M.; Freeman, B. D. Maximizing the right stuff: The trade-off between membrane permeability and selectivity. *Science* **2017**, *356* (6343), eaab0530. <https://doi.org/10.1126/science.aab0530>.
- (7) Yeo, J. Y.; Tapia, B. C.; Smith, Z. P. Understanding the effect of film thickness on the physical aging of highly microporous CANAL polymers for membrane-based gas separations. *In Prep* **2025**.
- (8) Guo, L.-P.; Liu, R.-S.; Qian, J.; Hao, G.-P.; Guo, J.; Wu, H.; Wang, F.; Lu, A.-H. Surface sieving carbon skins for propylene and propane separation. *Nat. Chem. Eng.* **2024**, *1* (6), 411–420. <https://doi.org/10.1038/s44286-024-00075-9>.
- (9) Christopher, C. C. E.; Dutta, A.; Farooq, S.; Karimi, I. A. Process synthesis and optimization of propylene/propane separation using vapor recompression and self-heat recuperation. *Ind. Eng. Chem. Res.* **2017**, *56* (49), 14557–14564. <https://doi.org/10.1021/acs.iecr.7b03432>.
- (10) Physical constants of organic compounds. In *CRC handbook of chemistry and physics*; Rumble, J. R., Ed.; CRC Press/Taylor & Francis: Boca Raton, FL.
- (11) Zhang, C.; Lively, R. P.; Zhang, K.; Johnson, J. R.; Karvan, O.; Koros, W. J. Unexpected molecular sieving properties of Zeolitic Imidazolate Framework-8. *J. Phys. Chem. Lett.* **2012**, *3* (16), 2130–2134. <https://doi.org/10.1021/jz300855a>.
- (12) Su, Y.; Cong, S.; Shan, M.; Zhang, Y. Enhanced propylene/propane separation in facilitated transport membranes containing multisilver complex. *AIChE J.* **2022**, *68* (1), e17410. <https://doi.org/10.1002/aic.17410>.
- (13) Chan, Y. H.; Lock, S. S. M.; Wong, M. K.; Yiin, C. L.; Loy, A. C. M.; Cheah, K. W.; Chai, S. Y. W.; Li, C.; How, B. S.; Chin, B. L. F.; Chan, Z. P.; Lam, S. S. A state-of-the-art review on capture and separation of hazardous hydrogen sulfide (H₂S): Recent advances, challenges and outlook. *Environ. Pollut.* **2022**, *314*, 120219. <https://doi.org/10.1016/j.envpol.2022.120219>.
- (14) Pudi, A.; Rezaei, M.; Signorini, V.; Andersson, M. P.; Baschetti, M. G.; Mansouri, S. S. Hydrogen sulfide capture and removal technologies: A comprehensive review of recent developments and emerging trends. *Sep. Purif. Technol.* **2022**, *298*, 121448. <https://doi.org/10.1016/j.seppur.2022.121448>.
- (15) Tengku Hassan, T. N. A.; Shariff, A. M.; Mohd Pauzi, M. M.; Khidzir, M. S.; Surmi, A. Insights on Cryogenic Distillation Technology for Simultaneous CO₂ and H₂S Removal for Sour Gas Fields. *Molecules* **2022**, *27* (4), 1424. <https://doi.org/10.3390/molecules27041424>.



- (16) Torres, F. B.; Gutierrez, J. P.; Ruiz, L. A.; Bertuzzi, M. A.; Erdmann, E. Comparative analysis of absorption, membrane, and hybrid technologies for CO₂ recovery. *J. Nat. Gas Sci. Eng.* **2021**, *94*, 104082. <https://doi.org/10.1016/j.jngse.2021.104082>.
- (17) He, X.; Chen, D.; Liang, Z.; Yang, F. Insight and comparison of energy-efficient membrane processes for CO₂ capture from flue gases in power plant and energy-intensive industry. *Carbon Capture Sci. Technol.* **2022**, *2*, 100020. <https://doi.org/10.1016/j.ccs.2021.100020>.
- (18) Mizrahi Rodriguez, K.; Lin, S.; Wu, A. X.; Storme, K. R.; Joo, T.; Grosz, A. F.; Roy, N.; Syar, D.; Benedetti, F. M.; Smith, Z. P. Penetrant-induced plasticization in microporous polymer membranes. *Chem. Soc. Rev.* **2024**, *53* (5), 2435–2529. <https://doi.org/10.1039/d3cs00235g>.
- (19) Sholl, D. S.; Lively, R. P. Exemplar mixtures for studying complex mixture effects in practical chemical separations. *JACS Au* **2022**, *2* (2), 322–327. <https://doi.org/10.1021/jacsau.1c00490>.
- (20) Yeo, J. Y.; Benedetti, F. M.; Pedretti, B.; Robinson, A. M.; Yin, R.; Lai, H. W. H.; Lee, T. H.; Xia, Y.; Smith, Z. P. Investigation of competitive sorption and plasticization of hyperaged CANAL ladder polymers for acid gas purification. *J. Membr. Sci.* **2025**, 123973. <https://doi.org/10.1016/j.memsci.2025.123973>.
- (21) Yi, S.; Ma, X.; Pinnau, I.; Koros, W. J. A high-performance hydroxyl-functionalized polymer of intrinsic microporosity for an environmentally attractive membrane-based approach to decontamination of sour natural gas. *J. Mater. Chem. A* **2015**, *3* (45), 22794–22806. <https://doi.org/10.1039/c5ta05928c>.
- (22) Yi, S.; Ghanem, B.; Liu, Y.; Pinnau, I.; Koros, W. J. Ultrasensitive glassy polymer membranes with unprecedented performance for energy-efficient sour gas separation. *Sci. Adv.* **2019**, *5* (5). <https://doi.org/10.1126/sciadv.aaw5459>.
- (23) Dean, P. A.; Mizrahi Rodriguez, K.; Guo, S.; Roy, N.; Swager, T. M.; Smith, Z. P. Elucidating the role of micropore-generating backbone motifs and amine functionality on H₂S, CO₂, CH₄ and N₂ sorption. *J. Membr. Sci.* **2024**, *696*, 122465. <https://doi.org/10.1016/j.memsci.2024.122465>.
- (24) Mizrahi Rodriguez, K.; Dean, P. A.; Guo, S.; Roy, N.; Swager, T. M.; Smith, Z. P. Elucidating the role of micropore-generating backbone motifs and amine functionality on membrane separation performance in complex mixtures. *J. Membr. Sci.* **2024**, *696*, 122464. <https://doi.org/10.1016/j.memsci.2024.122464>.
- (25) Paul, D. R. Effect of immobilizing adsorption on the diffusion time lag. *J. Polym. Sci., Part A-2: Polym. Phys.* **1969**, *7* (10), 1811–1818. <https://doi.org/10.1002/pol.1969.160071015>.
- (26) Fredrickson, G. H.; Helfand, E. Dual-mode transport of penetrants in glassy polymers. *Macromolecules* **1985**, *18* (11), 2201–2207. <https://doi.org/10.1021/ma00153a024>.
- (27) Kanehashi, S.; Nagai, K. Analysis of dual-mode model parameters for gas sorption in glassy polymers. *J. Membr. Sci.* **2005**, *253* (1), 117–138. <https://doi.org/10.1016/j.memsci.2005.01.003>.
- (28) Koros, W. J.; Chern, R. T.; Stannett, V.; Hopfenberg, H. B. A model for permeation of mixed gases and vapors in glassy polymers. *J. Polym. Sci.: Polym. Phys. Ed.* **1981**, *19* (10), 1513–1530. <https://doi.org/10.1002/pol.1981.180191004>.
- (29) Ricci, E.; De Angelis, M. G. Modelling mixed-gas sorption in glassy polymers for CO₂ removal: a sensitivity analysis of the dual mode sorption model. *Membranes* **2019**, *9* (1), 8. <https://doi.org/10.3390/membranes9010008>.
- (30) Wu, A. X.; Drayton, J. A.; Mizrahi Rodriguez, K.; Benedetti, F. M.; Qian, Q.; Lin, S.; Smith, Z. P. Elucidating the role of fluorine content on gas sorption properties of fluorinated polyimides. *Macromolecules* **2021**, *54* (1), 22–34. <https://doi.org/10.1021/acs.macromol.0c01746>.



- (31) Barrer, R. M.; Barrie, J. A.; Raman, N. K. Solution and diffusion in silicone rubber I—A comparison with natural rubber. *Polymer* **1962**, *3*, 595–603. [https://doi.org/10.1016/0032-3861\(62\)90108-8](https://doi.org/10.1016/0032-3861(62)90108-8).
- (32) Smith, Z. P.; Tiwari, R. R.; Murphy, T. M.; Sanders, D. F.; Gleason, K. L.; Paul, D. R.; Freeman, B. D. Hydrogen sorption in polymers for membrane applications. *Polymer* **2013**, *54* (12), 3026–3037. <https://doi.org/10.1016/j.polymer.2013.04.006>.
- (33) Koros, W. J.; Paul, D. R.; Huvard, G. S. Energetics of gas sorption in glassy polymers. *Polymer* **1979**, *20* (8), 956–960. [https://doi.org/10.1016/0032-3861\(79\)90192-7](https://doi.org/10.1016/0032-3861(79)90192-7).
- (34) Abbott, L. J.; Hart, K. E.; Colina, C. M. Polymatic: a generalized simulated polymerization algorithm for amorphous polymers. *Theor. Chem. Acc.* **2013**, *132* (3), 1334. <https://doi.org/10.1007/s00214-013-1334-z>.
- (35) Larsen, G. S.; Lin, P.; Hart, K. E.; Colina, C. M. Molecular simulations of PIM-1-like polymers of intrinsic microporosity. *Macromolecules* **2011**, *44* (17), 6944–6951. <https://doi.org/10.1021/ma200345v>.
- (36) Abbott, L.; Colina, C. Polymatic: a simulated polymerization algorithm, 2013. <https://nanohub.org/resources/17278> (accessed 2024-11-21).
- (37) Morgan, W. J.; Anstine, D. M.; Colina, C. M. Temperature effects in flexible adsorption processes for amorphous microporous polymers. *J. Phys. Chem. B* **2022**, *126* (33), 6354–6365. <https://doi.org/10.1021/acs.jpcc.2c04543>.
- (38) Kupgan, G.; Demidov, A. G.; Colina, C. M. Plasticization behavior in polymers of intrinsic microporosity (PIM-1): A simulation study from combined Monte Carlo and molecular dynamics. *J. Membr. Sci.* **2018**, *565*, 95–103. <https://doi.org/10.1016/j.memsci.2018.08.004>.
- (39) Anstine, D. M.; Demidov, A. G.; Mendez, N. F.; Morgan, W. J.; Colina, C. M. Screening PIM-1 performance as a membrane for binary mixture separation of gaseous organic compounds. *J. Membr. Sci.* **2020**, *599*, 117798. <https://doi.org/10.1016/j.memsci.2019.117798>.
- (40) Kupgan, G.; Liyana-Arachchi, T. P.; Colina, C. M. NLDFT pore size distribution in amorphous microporous materials. *Langmuir* **2017**, *33* (42), 11138–11145. <https://doi.org/10.1021/acs.langmuir.7b01961>.
- (41) Theodorou, D. N.; Suter, U. W. Detailed molecular structure of a vinyl polymer glass. *Macromolecules* **1985**, *18* (7), 1467–1478. <https://doi.org/10.1021/ma00149a018>.
- (42) Thompson, A. P.; Aktulga, H. M.; Berger, R.; Bolintineanu, D. S.; Brown, W. M.; Crozier, P. S.; in 't Veld, P. J.; Kohlmeyer, A.; Moore, S. G.; Nguyen, T. D.; Shan, R.; Stevens, M. J.; Tranchida, J.; Trott, C.; Plimpton, S. J. LAMMPS - a flexible simulation tool for particle-based materials modeling at the atomic, meso, and continuum scales. *Comput. Phys. Commun.* **2022**, *271*, 108171. <https://doi.org/10.1016/j.cpc.2021.108171>.
- (43) Martin, M. G.; Siepmann, J. I. Transferable potentials for phase equilibria. 1. United-atom description of n-alkanes. *J. Phys. Chem. B* **1998**, *102* (14), 2569–2577. <https://doi.org/10.1021/jp972543+>.
- (44) Martin, M. G.; Siepmann, J. I. Novel configurational-bias Monte Carlo method for branched molecules. Transferable potentials for phase equilibria. 2. United-atom description of branched alkanes. *J. Phys. Chem. B* **1999**, *103* (21), 4508–4517. <https://doi.org/10.1021/jp984742e>.
- (45) Lee, J.-S.; Wick, C. D.; Stubbs, J. M.; Siepmann, J. I. Simulating the vapour–liquid equilibria of large cyclic alkanes. *Mol. Phys.* **2005**, *103* (1), 99–104. <https://doi.org/10.1080/00268970412331303341>.



- (46) Wang, J.; Wolf, R. M.; Caldwell, J. W.; Kollman, P. A.; Case, D. A. Development and testing of a general Amber force field. *J. Comput. Chem.* **2004**, *25* (9), 1157–1174. <https://doi.org/10.1002/jcc.20035>.
- (47) He, X.; Man, V. H.; Yang, W.; Lee, T.-S.; Wang, J. A fast and high-quality charge model for the next generation general AMBER force field. *J. Chem. Phys.* **2020**, *153* (11), 114502. <https://doi.org/10.1063/5.0019056>.
- (48) Potoff, J. J.; Siepmann, J. I. Vapor–liquid equilibria of mixtures containing alkanes, carbon dioxide, and nitrogen. *AIChE J.* **2001**, *47* (7), 1676–1682. <https://doi.org/10.1002/aic.690470719>.
- (49) Zhang, L.; Siepmann, J. I. Direct calculation of Henry's law constants from Gibbs ensemble Monte Carlo simulations: nitrogen, oxygen, carbon dioxide and methane in ethanol. *Theor. Chem. Acc.* **2006**, *115* (5), 391–397. <https://doi.org/10.1007/s00214-005-0073-1>.
- (50) Bayly, C. I.; Cieplak, P.; Cornell, W.; Kollman, P. A. A well-behaved electrostatic potential based method using charge restraints for deriving atomic charges: the RESP model. *J. Phys. Chem.* **1993**, *97* (40), 10269–10280. <https://doi.org/10.1021/j100142a004>.
- (51) Vanquelef, E.; Simon, S.; Marquant, G.; Garcia, E.; Klimerek, G.; Delepine, J. C.; Cieplak, P.; Dupradeau, F.-Y. R.E.D. Server: a web service for deriving RESP and ESP charges and building force field libraries for new molecules and molecular fragments. *Nucleic Acids Res.* **2011**, *39*, W511–W517. <https://doi.org/10.1093/nar/gkr288>.
- (52) Frisch, M. J.; Trucks, G. W.; Schlegel, H. B.; Scuseria, G. E.; Robb, M. A.; Cheeseman, J. R.; Scalmani, G.; Barone, V.; Petersson, G. A.; Nakatsuji, H.; Li, X.; Caricato, M.; Marenich, A. V.; Bloino, J.; Janesko, B. G.; Gomperts, R.; Mennucci, B.; Hratchian, H. P.; Ortiz, J. V.; Izmaylov, A. F.; Sonnenberg, J. L.; Williams, D. J.; Ding, F.; Lipparini, F.; Egidi, F.; Goings, J.; Peng, B.; Petrone, A.; Henderson, T.; Ranasinghe, D.; Zakrzewski, V. G.; Gao, J.; Rega, N.; Zheng, G.; Liang, W.; Hada, M.; Ehara, M.; Toyota, K.; Fukuda, R.; Hasegawa, J.; Ishida, M.; Nakajima, T.; Honda, Y.; Kitao, O.; Nakai, H.; Vreven, T.; Throssell, K.; Montgomery Jr., J. A.; Peralta, J. E.; Ogliaro, F.; Bearpark, M. J.; Heyd, J. J.; Brothers, E. N.; Kudin, K. N.; Staroverov, V. N.; Keith, T. A.; Kobayashi, R.; Normand, J.; Raghavachari, K.; Rendell, A. P.; Burant, J. C.; Iyengar, S. S.; Tomasi, J.; Cossi, M.; Millam, J. M.; Klene, M.; Adamo, C.; Cammi, R.; Ochterski, J. W.; Martin, R. L.; Morokuma, K.; Farkas, O.; Foresman, J. B.; Fox, D. J. Gaussian 16 Rev. C.01, 2016.
- (53) Dupradeau, F.-Y.; Pigache, A.; Zaffran, T.; Savineau, C.; Lelong, R.; Grivel, N.; Lelong, D.; Rosanski, W.; Cieplak, P. The R.E.D. tools: advances in RESP and ESP charge derivation and force field library building. *Phys. Chem. Chem. Phys.* **2010**, *12* (28), 7821–7839. <https://doi.org/10.1039/c0cp00111b>.
- (54) R.E.D. Python: Object oriented programming for Amber force fields. <https://www.morressier.com/o/event/5fc6334e03137aa5254ffe1e/article/5fc6341b9e0a135cbea5e93> (accessed 2024-11-21).
- (55) Connolly, M. L. Analytical molecular surface calculation. *J. Appl. Crystallogr.* **1983**, *16* (5), 548–558. <https://doi.org/10.1107/s0021889883010985>.
- (56) Davel, C. M.; Bernat, T.; Wagner, J. R.; Shirts, M. R. Parameterization of general organic polymers within the open force field framework. *J. Chem. Inf. Model.* **2024**, *64* (4), 1290–1305. <https://doi.org/10.1021/acs.jcim.3c01691>.
- (57) Patel, S.; Brooks III, C. L. CHARMM fluctuating charge force field for proteins: I parameterization and application to bulk organic liquid simulations. *J. Comput. Chem.* **2004**, *25* (1), 1–16. <https://doi.org/10.1002/jcc.10355>.



- (58) Teja, A. S.; Lee, R. J.; Rosenthal, D.; Anselme, M. Correlation of the critical properties of alkanes and alkanols. *Fluid Phase Equilib.* **1990**, *56*, 153–169. [https://doi.org/10.1016/0378-3812\(90\)85100-o](https://doi.org/10.1016/0378-3812(90)85100-o).
- (59) Maitland, G. C.; Rigby, M.; Smith, B.; Wakeham, W. A. *Intermolecular forces: their origin and determination*; International series of monographs on chemistry; Oxford University Press: Oxford, 1987.
- (60) Hockney, R. W.; Eastwood, J. W. *Computer simulation using particles*; CRC Press, 1988. <https://doi.org/10.1201/9780367806934>.
- (61) Homogeneous flows for atomic fluids: theory. In *Nonequilibrium molecular dynamics: Theory, algorithms and applications*; Todd, B. D., Daivis, P. J., Eds.; Cambridge University Press: Cambridge, 2017; pp 104–149. <https://doi.org/10.1017/9781139017848.006>.
- (62) Hoover, W. G. Canonical dynamics: equilibrium phase-space distributions. *Phys. Rev. A* **1985**, *31* (3), 1695–1697. <https://doi.org/10.1103/physreva.31.1695>.
- (63) Nosé, S. A unified formulation of the constant temperature molecular dynamics methods. *J. Chem. Phys.* **1984**, *81* (1), 511–519. <https://doi.org/10.1063/1.447334>.
- (64) Nosé, S. A molecular dynamics method for simulations in the canonical ensemble. *Mol. Phys.* **1984**, *52* (2), 255–268. <https://doi.org/10.1080/00268978400101201>.
- (65) Tuckerman, M.; Berne, B. J.; Martyna, G. J. Reversible multiple time scale molecular dynamics. *J. Chem. Phys.* **1992**, *97* (3), 1990–2001. <https://doi.org/10.1063/1.463137>.
- (66) Verlet, L. Computer “experiments” on classical fluids. I. Thermodynamical properties of Lennard-Jones molecules. *Phys. Rev.* **1967**, *159* (1), 98–103. <https://doi.org/10.1103/physrev.159.98>.
- (67) Yang, Q.; Zhong, C. Molecular simulation of adsorption and diffusion of hydrogen in metal–organic frameworks. *J. Phys. Chem. B* **2005**, *109* (24), 11862–11864. <https://doi.org/10.1021/jp051903n>.
- (68) Barraco, M.; Neyertz, S.; Benes, N. E.; Brown, D. Comparison of eight classical Lennard-Jones-based H₂ molecular models in the gas phase at temperatures and pressures relevant to hydrogen on-board storage tanks. *J. Phys. Chem. A* **2023**, *127* (30), 6335–6346. <https://doi.org/10.1021/acs.jpca.3c03212>.
- (69) Shah, M. S.; Tsapatsis, M.; Siepmann, J. I. Development of the transferable potentials for phase equilibria model for hydrogen sulfide. *J. Phys. Chem. B* **2015**, *119* (23), 7041–7052. <https://doi.org/10.1021/acs.jpcc.5b02536>.
- (70) Shah, J. K.; Marin-Rimoldi, E.; Mullen, R. G.; Keene, B. P.; Khan, S.; Paluch, A. S.; Rai, N.; Romaniello, L. L.; Rosch, T. W.; Yoo, B.; Maginn, E. J. Cassandra: An open source Monte Carlo package for molecular simulation. *J. Comput. Chem.* **2017**, *38* (19), 1727–1739. <https://doi.org/10.1002/jcc.24807>.
- (71) Fortunato, M. E.; Demidov, A. G.; Lin, S.; Tapia, B. C.; Lin, P.; Leon, K.; Perera, B. L. A.; Colina, C. M. SmithLabMIT/pysimm: v1.1.1, 2025. <https://doi.org/10.5281/zenodo.17247184>.
- (72) Fortunato, M. E.; Demidov, A. G.; Lin, S.; Lin, P.; Kwan, L.; Perera, B. L. A.; Colina, C. M. polysimtools/pysimm, 2024. <https://github.com/polysimtools/pysimm> (accessed 2024-11-21).
- (73) Fortunato, M. E.; Colina, C. M. *pysimm*: A python package for simulation of molecular systems. *SoftwareX* **2017**, *6*, 7–12. <https://doi.org/10.1016/j.softx.2016.12.002>.
- (74) Demidov, A. G.; Fortunato, M. E.; Colina, C. M. Update 0.2 to “pysimm: A Python package for simulation of molecular systems.” *SoftwareX* **2018**, *7*, 70–73. <https://doi.org/10.1016/j.softx.2018.02.006>.



- (75) Demidov, A. G.; Perera, B. L. A.; Fortunato, M. E.; Lin, S.; Colina, C. M. Update 1.1 to “pysimm: A Python package for simulation of molecular systems.” *SoftwareX* **2021**, *15*, 100749. <https://doi.org/10.1016/j.softx.2021.100749>.
- (76) Bevington, P. R.; Robinson, D. K. *Data reduction and error analysis for the physical sciences*; McGraw-Hill, 2003.
- (77) Neyertz, S.; Brown, D. Single- and mixed-gas sorption in large-scale molecular models of glassy bulk polymers. Competitive sorption of a binary CH₄/N₂ and a ternary CH₄/N₂/CO₂ mixture in a polyimide membrane. *J. Membr. Sci.* **2020**, *614*, 118478. <https://doi.org/10.1016/j.memsci.2020.118478>.
- (78) Schneider, C. A.; Rasband, W. S.; Eliceiri, K. W. NIH Image to ImageJ: 25 years of image analysis. *Nat. Methods* **2012**, *9* (7), 671–675. <https://doi.org/10.1038/nmeth.2089>.
- (79) Hansen, P. C.; O’Leary, D. P. The use of the L-curve in the regularization of discrete ill-posed problems. *SIAM J. Sci. Comput.* **1993**, *14* (6), 1487–1503. <https://doi.org/10.1137/0914086>.
- (80) Mizrahi Rodriguez, K.; Benedetti, F. M.; Roy, N.; Wu, A. X.; Smith, Z. P. Sorption-enhanced mixed-gas transport in amine functionalized polymers of intrinsic microporosity (PIMs). *J. Mater. Chem. A* **2021**, *9* (41), 23631–23642. <https://doi.org/10.1039/d1ta06530k>.
- (81) Sarkisov, L.; Bueno-Perez, R.; Sutharson, M.; Fairen-Jimenez, D. Materials informatics with PoreBlazer v4.0 and the CSD MOF database. *Chem. Mater.* **2020**, *32* (23), 9849–9867. <https://doi.org/10.1021/acs.chemmater.0c03575>.
- (82) Shieh, J.-J.; Chung, T. S. Gas permeability, diffusivity, and solubility of poly(4-vinylpyridine) film. *J. Polym. Sci., Part B: Polym. Phys.* **1999**, *37* (20), 2851–2861. [https://doi.org/10.1002/\(SICI\)1099-0488\(19991015\)37:20%253C2851::AID-POLB5%253E3.0.CO;2-U](https://doi.org/10.1002/(SICI)1099-0488(19991015)37:20%253C2851::AID-POLB5%253E3.0.CO;2-U).
- (83) Lodge, T.; Hiemenz, P. C. *Polymer chemistry*, 3rd edition.; CRC Press, Taylor & Francis Group, 2020.
- (84) Tang, Z.; Okazaki, S. All-atomistic molecular dynamics study of the glass transition of amorphous polymers. *Polymer* **2022**, *254*, 125044. <https://doi.org/10.1016/j.polymer.2022.125044>.
- (85) Klajmon, M.; Aulich, V.; Ludík, J.; Červinka, C. Glass transition and structure of organic polymers from all-atom molecular simulations. *Ind. Eng. Chem. Res.* **2023**, *62* (49), 21437–21448. <https://doi.org/10.1021/acs.iecr.3c03038>.
- (86) Sharma, P.; Roy, S.; Karimi-Varzaneh, H. A. Validation of force fields of rubber through glass-transition temperature calculation by microsecond atomic-scale molecular dynamics simulation. *J. Phys. Chem. B* **2016**, *120* (7), 1367–1379. <https://doi.org/10.1021/acs.jpcc.5b10789>.
- (87) Han, J.; Gee, R. H.; Boyd, R. H. Glass transition temperatures of polymers from molecular dynamics simulations. *Macromolecules* **1994**, *27* (26), 7781–7784. <https://doi.org/10.1021/ma00104a036>.
- (88) Lyulin, A. V.; Balabaev, N. K.; Michels, M. A. J. Molecular-weight and cooling-rate dependence of simulated T_g for amorphous polystyrene. *Macromolecules* **2003**, *36* (22), 8574–8575. <https://doi.org/10.1021/ma034406i>.
- (89) Karuth, A.; Alesadi, A.; Xia, W.; Rasulev, B. Predicting glass transition of amorphous polymers by application of cheminformatics and molecular dynamics simulations. *Polymer* **2021**, *218*, 123495. <https://doi.org/10.1016/j.polymer.2021.123495>.
- (90) Paul, W.; Smith, G. D. Structure and dynamics of amorphous polymers: computer simulations compared to experiment and theory. *Rep. Prog. Phys.* **2004**, *67* (7), 1117. <https://doi.org/10.1088/0034-4885/67/7/r03>.
- (91) Dubrovinsky, L. Thermal expansion and equation of state. In *Encyclopedia of materials: Science and technology*; Buschow, K. H. J., Cahn, R. W., Flemings, M. C., Ilshner, B., Kramer, E. J.,



- Mahajan, S., Veyssière, P., Eds.; Elsevier: Oxford, 2002; pp 1–4. <https://doi.org/10.1016/b0-08-043152-6/01817-9>.
- (92) Grulke, E. A.; Bloch, D. R.; Akihiro, A.; Brandrup, J.; Edmund H Immergut. Physical constants of some important polymers. In *Polymer handbook*; John Wiley & Sons, 1999.
- (93) Clash, R. F. Jr.; Rynkiewicz, L. M. Thermal expansion properties of plastic materials. *Ind. Eng. Chem.* **1944**, *36* (3), 279–282. <https://doi.org/10.1021/ie50411a021>.
- (94) Yamato, M.; Imai, A.; Kawakami, H. Thermal properties of polymer with intrinsic microporosity membranes. *Polymer* **2022**, *259*, 125339. <https://doi.org/10.1016/j.polymer.2022.125339>.
- (95) Seaton, N. A.; Walton, J. P. R. B.; Quirke, N. A new analysis method for the determination of the pore size distribution of porous carbons from nitrogen adsorption measurements. *Carbon* **1989**, *27* (6), 853–861. [https://doi.org/10.1016/0008-6223\(89\)90035-3](https://doi.org/10.1016/0008-6223(89)90035-3).
- (96) Lastoskie, C.; Gubbins, K. E.; Quirke, N. Pore size distribution analysis of microporous carbons: a density functional theory approach. *J. Phys. Chem.* **1993**, *97* (18), 4786–4796. <https://doi.org/10.1021/j100120a035>.
- (97) Peng, H.-G.; Vallery, R. S.; Liu, M.; Skalsey, M.; Gidley, D. W. Depth-profiled positronium annihilation lifetime spectroscopy on porous films. *Colloids Surf. A Physicochem. Eng. Asp.* **2007**, *300* (1), 154–161. <https://doi.org/10.1016/j.colsurfa.2006.10.072>.
- (98) Hou, R.; D. Smith, S. J.; Konstas, K.; M. Doherty, C.; D. Easton, C.; Park, J.; Yoon, H.; Wang, H.; D. Freeman, B.; R. Hill, M. Synergistically improved PIM-1 membrane gas separation performance by PAF-1 incorporation and UV irradiation. *J. Mater. Chem. A* **2022**, *10* (18), 10107–10119. <https://doi.org/10.1039/d2ta00138a>.
- (99) Le Roux, S.; Petkov, V. ISAACS – interactive structure analysis of amorphous and crystalline systems. *J. Appl. Crystallogr.* **2010**, *43* (1), 181–185. <https://doi.org/10.1107/s0021889809051929>.
- (100) Makowski, L. Characterization of proteins with wide-angle X-ray solution scattering (WAXS). *J. Struct. Funct. Genomics* **2010**, *11* (1), 9–19. <https://doi.org/10.1007/s10969-009-9075-x>.
- (101) Canti, L. Theoretical modeling of gas adsorption in microporous aromatic polymers, University of Eastern Piedmont, Vercelli, Italy, 2016. <https://doi.org/10.20373/uniupo/openthesis/81935>.
- (102) Yoshimoto, Y.; Tomita, Y.; Sato, K.; Higashi, S.; Yamato, M.; Takagi, S.; Kawakami, H.; Kinefuchi, I. Gas adsorption and diffusion behaviors in interfacial systems composed of a polymer of intrinsic microporosity and amorphous silica: a molecular simulation study. *Langmuir* **2022**, *38* (24), 7567–7579. <https://doi.org/10.1021/acs.langmuir.2c00661>.
- (103) Dymond, J. H.; Wilhoit, R. C.; Marsh, K. N.; Wong, K. C. *Virial coefficients of pure gases*; Frenkel, M., Marsh, K. N., Eds.; Landolt-Börnstein - Group IV Physical Chemistry; Springer-Verlag: Berlin/Heidelberg, 2002; Vol. 21A. <https://doi.org/10.1007/b71692>.
- (104) Linstrom, P. J.; Mallard, W. G. The NIST Chemistry WebBook: A chemical data resource on the internet. *J. Chem. Eng. Data* **2001**, *46* (5), 1059–1063. <https://doi.org/10.1021/je000236i>.
- (105) Peng, D.-Y.; Robinson, D. B. A new two-constant equation of state. *Ind. Eng. Chem. Fundam.* **1976**, *15* (1), 59–64. <https://doi.org/10.1021/i160057a011>.
- (106) Balçık, M.; Tantekin-Ersolmaz, S. B.; Pinnau, I.; Ahunbay, M. G. CO₂/CH₄ mixed-gas separation in PIM-1 at high pressures: Bridging atomistic simulations with process modeling. *J. Membr. Sci.* **2021**, *640*, 119838. <https://doi.org/10.1016/j.memsci.2021.119838>.
- (107) Lee, T. H.; Smith, Z. P. Better standards are needed for membrane materials. *Nat. Mater.* **2024**, *23* (1), 11–12. <https://doi.org/10.1038/s41563-023-01763-2>.



- (108) Neyertz, S.; Benes, N. E.; Brown, D. Molecular simulations of hybrid cross-linked membranes for H₂S gas separation at very high temperatures and pressure: Binary 90%/10% N₂/H₂S and CH₄/H₂S, ternary 90%/9%/1% N₂/CO₂/H₂S and CH₄/CO₂/H₂S mixtures. *J. Membr. Sci.* **2023**, *687*, 122092. <https://doi.org/10.1016/j.memsci.2023.122092>.
- (109) Yeo, J. Y.; Tapia, B. C.; Benedetti, F. M.; Robinson, A. M.; Richardson, J.; Pedretti, B. J.; Lee, T. H.; Freeman, B. D.; Xia, Y.; Smith, Z. P. Ultra-selective CANAL polymers for hydrogen-based membrane separations after long-term aging. *Journal of Membrane Science* **2025**, 125038. <https://doi.org/10.1016/j.memsci.2025.125038>.
- (110) Koros, W. J.; Paul, D. R. CO₂ sorption in poly(ethylene terephthalate) above and below the glass transition. *J. Polym. Sci.: Polym. Phys. Ed.* **1978**, *16* (11), 1947–1963. <https://doi.org/10.1002/pol.1978.180161105>.
- (111) Tofallis, C. A better measure of relative prediction accuracy for model selection and model estimation. *J. Oper. Res. Soc.* **2015**, *66* (8), 1352–1362. <https://doi.org/10.1057/jors.2014.103>.
- (112) Yoshimizu, H.; Ohta, S.; Asano, T.; Suzuki, T.; Tsujita, Y. Temperature dependence of the mean size of polyphenyleneoxide microvoids, as studied by Xe sorption and ¹²⁹Xe NMR chemical shift analyses. *Polym. J.* **2012**, *44* (8), 821–826. <https://doi.org/10.1038/pj.2012.123>.
- (113) Li, P.; Chung, T. S.; Paul, D. R. Temperature dependence of gas sorption and permeation in PIM-1. *J. Membr. Sci.* **2014**, *450*, 380–388. <https://doi.org/10.1016/j.memsci.2013.09.030>.
- (114) Nelson, R. D.; Lide, D. R.; Maryott, A. A. *Selected values of electric dipole moments for molecules in the gas phase*; National standards reference data series; NSRDS-NBS 10; National Institute of Standards and Technology: Gaithersburg, MD, 1967. <https://www.nist.gov/publications/selected-values-electric-dipole-moments-molecules-gas-phase>.
- (115) Chen, B. W. C.; O'Brien, C. P. Highly selective propylene/propane separation using amine-modified PIM-1 (PIM-NH₂). *J. Membr. Sci.* **2025**, *731*, 124229. <https://doi.org/10.1016/j.memsci.2025.124229>.
- (116) Kuah, W. C.; Effendy, S.; Farooq, S. Industrial scale propylene/propane separation using pressure vacuum swing adsorption. *Ind. Eng. Chem. Res.* **2018**, *57* (18), 6451–6463. <https://doi.org/10.1021/acs.iecr.8b00289>.
- (117) Sridhar, S.; Khan, A. A. Simulation studies for the separation of propylene and propane by ethylcellulose membrane. *J. Membr. Sci.* **1999**, *159* (1), 209–219. [https://doi.org/10.1016/s0376-7388\(99\)00061-7](https://doi.org/10.1016/s0376-7388(99)00061-7).



Data Availability Statement for

**Computational and experimental insights into variable temperature
propylene (C₃H₆), propane (C₃H₈), and hydrogen sulfide (H₂S) sorption in
ultra-high permselectivity CANAL ladder polymers**

Brandon C. Tapia¹, Jing Ying Yeo¹, and Zachary P. Smith^{*1}

¹Department of Chemical Engineering, Massachusetts Institute of Technology, Cambridge, Massachusetts
02139, USA

*Corresponding author: Zachary P. Smith (zpsmith@mit.edu)

The data supporting this article have been included as part of the Supplementary Information.

